INFN

# ISTITUTO NAZIONALE DI FISICA NUCLEARE

**Laboratori Nazionali del Sud**

**INFN/TC-02/06**
**4 April 2002**

## THE ECLISSE EXPERIMENT: PRODUCTION OF HIGH INTENSITY ION BEAMS BY MEANS OF A HYBRID ION SOURCE

S. Gammino[1)], L. Torrisi[1)], L. Andò[1)], G. Ciavola[1)], L. Celona[1)], S. Genovese[1)], A. M. Mezzasalma[2)], J. Krása[3)], L.Láska[3)], M. Pfeifer[3)], K. Rohlena[3)], E. Woryna[4)], J. Wolowski[4)], P. Parys[4)], G.D. Shirkov[5)], V. Mironov[5)]

*1) INFN-LNS, Via S. Sofia 44, 95123 Catania, Italy*
*2) Dip. di Fisica della Materia e Tecnologie Fisiche Avanzate, Università di Messina Ctr. Papardo-Sperone 31, S.Agata-Messina, Italy*
*3) Institute of Physics-ASCR, Na Slovance 2, Prague, Czech Republic*
*4) Institute of Plasma Physics and Laser Microfusion, Hery Street, Warsaw, Poland*
*5) Joint Institute for Nuclear Research-Laboratory of Particle Physics, Dubna, Russia*

**Abstract**

The ECLISSE project (ECR ion source Coupled to a Laser Ion Source for charge State Enhancement) started in 1999 with the aim to obtain intense beam of highly charged ions (pulsed mode) by means of the coupling between a Laser Ion Source (LIS) and an electron cyclotron resonance (ECR) ion source. The major points to be investigated appeared to be the coupling efficiency of the ion beam produced by the LIS to the ECR plasma, as well as the possibility to enhance the available charge state by an ECRIS with respect to the standard methods used now to produce ion beams from solid samples (i.e. evaporation and sputtering). The theory suggests that this concept may be effective, provided that the ion energy from the LIS is of the order of a few hundreds of eV. The main features of the theory will be shown in the following, along with the results obtained in the off-line test at LNS facility (Nd:YAG laser 0.9 J / 9 ns, laser power densities < $10^{11}$ W/cm$^2$) and at IPPLM facility (Nd:glass laser 10 J / 1 ns, limited to 1.5 J).

PACS.: 41.75.Ak; 52.58.-r; 52.50.Jm; 29.25.Ni

*Published by* ***SIS–Pubblicazioni***
*Laboratori Nazionali di Frascati*

## 1 INTRODUCTION

The possibility to produce intense metal ion beams, pulsed or dc mode, by means of an hybrid source, consisting of a Laser Ion Source (LIS) as the 1st stage and of an Electron Cyclotron Resonance Ion Source (ECRIS) as the 2nd stage, is under study at the Laboratori Nazionali del Sud (LNS).

A collaboration was established in 1999 with IPPLM, Warsaw, IP-ASCR Prague and JINR-LPP Dubna aimed to study:

- the efficiency of the coupling process of ions from the LIS beam to the ECRIS plasma;
- the plasma behavior and the charge state distribution (CSD) that can be produced by the hybrid ion source;
- the ion charge state distribution as a function of the LIS-produced ion energy;
- the effect of the magnetic field on LIS output;
- the effect of biasing the metal target;
- the energy distribution and CSD produced by the LIS at different laser power density;
- the etching rates and the amount of the ionic and neutral components extracted from the target;
- the reproducibility and stability of LIS.

The concept of the hybrid ion source is simple: the first stage of the hybrid ion source will give intense currents of electrons and of multiply charged ions ($q/m$ = 1/10 or lower), then the ECR ion source will act as a charge state multiplier. The idea of this new type of ion source [1], as well as the results of the preliminary experiments, were presented elsewhere [2-6].

The experiments have been carried out either at IPPLM and at LNS.

The aim of the experiments at LNS consisted of the minimization of the energy of multiply charged ions, of the maximization of the emitted ion current and of the study of etching rates at high repetition rates of the laser.

The experimental facility is shown in figs. 1 (scheme of the irradiation vacuum chamber) and 2 (photo of the experimental area).

Tab. 1 shows the main characteristics of the laser and of the LIS and tab. 2 presents the main features of the superconducting SERSE source which will be used for the on-line tests, and its parameters which are used for the simulations.

The aim of the experiments at IPPLM with single shot laser consisted mainly of the study of the effect of the magnetic field and of the bias voltage on the ion emission from the target.

The facility at IPPLM is shown in fig. 3 and the parameter of the laser and of the LIS are given in tab. 3.

## 2 THE THEORETICAL FRAMEWORK

The main requirement for multicharged ion loading is that the ions should be slowed down and trapped in the ECR plasma.

The beam of heavy ions interacts with the plasma mostly as the result of elastic Coulomb collisions. Interaction with ions is much more effective in comparison with electrons due to the low mass of electrons and their high energy in the plasma. By using the theory of elastic Coulomb collisions in the plasma [7,8], the rate of energy loss $\frac{dE_i}{dx}$ of an ion beam of charge states $i$, atomic mass number $A_i$ and energy $E_i$ can be evaluated as it follows:

$$\frac{dE_i}{dx} = - p^{3/2} \frac{A_i}{A_k} i^2 k^2 \frac{m_e^2 c^4}{E_i} r_e^2 n_k L_n \qquad (1)$$

where $A_k$ and $k$ are atomic mass number and average charge state of ions in the plasma, $L_n$ » 15 is so called Coulomb logarithms; $r_e$ and $m_e$ are the classical radius and mass of electron; $n_k$ is the ion density in the plasma and $c$ is the velocity of light. According to this formula the mean free path $l$ of beam ions in the plasma is

$$l = \frac{E_i^2}{4p\ m_e^2 c^4 i^2 k^2 n_k Ln} \frac{A_k}{A_i + A_k} = \frac{e_i^2}{4p\ m_e^2 c^4 k\, n_e Ln} \frac{A_k}{A_i + A_k} \qquad (2)$$

with the ion energy per charge $e_i = E_i ▯ i$ and electron density in plasma $n_e = k\ n_k$. then the ion beam absorption by the plasma of $L$ length is estimated as follows

$$N_i = N_0 (1 - exp( -L ▯ l )) \qquad (3)$$

where L is the length of the plasma volume along the ion beam axis.

These formulas have been used to determine the coupling of metal ion beams produced by a LIS to an ECR plasma.

Fig. 4 presents the chromium ($A_i$ = 52) and gold ($A_i$ = 197) ion beam absorption in the oxygen plasma (we have considered $A_k$ = 18, being $^{18}$O the typical mixing gas for the heaviest ions production, $k$ =6, $n_e$ = 4 $10^{12}$ cm$^{-3}$, $L$ = 12 cm) for different ion energy per charge.

It must be underlined that the trend is quite similar for different ion species and that high coupling efficiency is obtained only for $e_I$ = 100 eV. The coupling efficiency is close to zero for $e_I$ =1 keV; this value sets an upper limit for $e_I$ of a few hundreds of eV.

Moreover it should be considered that the ion beam which stops in the plasma transfers its kinetic energy to the plasma. If the total ion number in the beam is determined as $N_i = 6.2 \cdot 10^{18}\ I\ t_i$ then the total beam energy (eV) will be:

$$E = 6.2 \cdot 10^{18}\ I\ t_i\ i\ e_I \qquad (4)$$

where $I$ is the current in A and $t_i$ is the pulse duration in s.

Beam ions interact mostly with the plasma ions and heat them. The initial total ion energy in the plasma of volume $V$ and ion temperature $T_i$ is

$$E_0 = T_i\ V\ n_e ▯ k \qquad (5)$$

The energy transfer from the beam to the plasma should be lower to avoid that the beam perturbs the plasma. Fig. 5 shows the total beam energy $E$ in terms of the ion beam energy per charge $e_i$ (the two lines are corresponding to a beam current I=0.1 A and 0.3 A) in comparison with the total energy of ions $E_0$ in the plasma which parameters are: $k$ = 6, $n_e$ = 4 $10^{12}$ $cm^{-3}$, $V$ = 600 $cm^3$, $T_i$ = 20 eV. A current of 100 mA can be tolerated up to energies of 300 eV. Thus the formula (3) sets a limit on the maximum energy per charge and the maximum acceptable current is determined by such parameter through the formula (5).

## 3 NUMERICAL SIMULATION OF ION INJECTION INTO THE ECR SOURCE

Processes of ion accumulation and production in the plasma of ECR ion sources can be described with a set of nonlinear differential balance equations for all ionic charge states, electrons and neutrals existing in the source. The complete set of balance equations for all possible charge states (including single and double ionization and charge exchange processes between neutrals and ions) is used in the model and given, for example, in Ref. [9,10]

The physical model and mathematical equations introduced in Ref. [9,10] are able to describe qualitatively and simulate quantitatively the processes of ion accumulation and production in the static and pulsed regimes of the ECR source operation. Unfortunately there are no data about experimental values of the electron energy and density for the plasma of the SERSE source [11] which will be used as test bench for the ECLISSE experiment. But the comparison of the experimental charge state distributions with the results of calculations (by using the rf power as the fitting parameter) can be used for the estimation of the electron energy and density in terms of the model.

The presented simulations have been made in the frame of the existing model which is not able to take into consideration all the processes as particle scattering, energy absorption and dissipation, plasma heating etc., which appear when an external beam of charged particles propagates through the plasma. Thus, the presented results represent the ion beam injection into the plasma volume under certain assumptions (essentially the beam should not transfer to the plasma a larger energy than its energy content which is the case if $e_I$ = 200 eV ).

Essentially the simulations have shown that the ECR plasma is a sort of low-pass filter in terms of the ion energy distribution. In this sense the hybrid source should work better with sources which magnetic field trap allows a high confinement and then a high energy content.

The following parameters of SERSE were used in the simulations:

- average mirror ratio equal to 4.0;
- plasma length of 12 cm and diameter of 7.5 cm (this estimation of plasma dimensions was made according to the dimension of resonance zone for the given values of field maximum and for the position of the extraction hole which is currently used);

- electron temperature was fixed at 10 keV (this assumption is an extrapolation from existing data and charge state distribution, since no plasma diagnostics is available for this source).

Calculations have been carried out for different metallic ions, and for the typical operating conditions of SERSE. For sake of simplicity, the injection of a constant flux of 0.1 A, 20 μs burst per pulse with a charge state equal to 2 was assumed in the calculations. The injection of other charge states up to $10^+$ was studied but the final CSD results to be quite the same.

It was assumed in the presented simulation that a pure oxygen plasma is created and stored up to the stable state with electron density of 4 to 5 $10^{12}$ $cm^{-3}$; rf power between 1500 and 2000 W was switched on 10 ms before the laser injection. Fig. 6 presents the results of calculations for chromium (Z=24) ion production with external injection into the plasma. The time dependence of ion extraction currents is shown for a few selected charge states ($16^+$,$18^+$, $20^+$ and $22^+$)after the plasma ignition ($t$ = 0) and ion beam injection ($t \approx 10$ ms). The repetition rate of ion injection was 30 ms that corresponds to the maximum repetition rate of the laser available at LNS.

It can be observed that the CSD of extracted ions is changing with the time and that the average charge state increases according to the step by step ionization of ions in the plasma. The development of CSD in time looks like propagation of a wave along the time axis. The CSD in every moment of time is not so broad as it is for the continuous ion loading into the source, as the process is more efficient in pulsed mode. The amplitude of extracted charge state with maximum current grows up at the first step of highly charged ion generation. But then the ion losses dominate in the source and the amplitude of extracted current goes down. It is possible to choose an optimum charge state with the maximum output current at the optimum time for the given element and the given plasma parameters. The maximum output current of the optimum charge state is several times higher in comparison with ordinary ECR source regimes due to a narrow CSD in the regime of pulsed injection.

Fig. 6 shows that the production of the highest charge states (e.g. $Cr^{22+}$) has almost a cw behavior because of relatively long time of production of these charged stages in comparison with the injection repetition rate. These results are interesting for cw accelerators. Similar results are obtained for rubidium (Z= 37, fig. 7) and gold (Z= 79, fig. 8).

## 4 THE LNS EXPERIMENTAL SETUP

A 900 mJ/ 9 ns Nd:YAG laser was used in our experiments; single pulse regime and 30 Hz repetition rate regime were used. Unfortunately during the most recent series of tests the maximum laser energy was not higher than about 300 mJ (as measured by the calorimeter with laser power/energy monitor), three times lower than in the previous measurements, but yet sufficient to study the low energy, low charge states production regime in which we are interested.

We observed that the divergence of the laser beam significantly changes with increasing laser energy and during the experiment, and it was a major obstacle to our experiment, because the evaluation of the laser beam spot and then of the effective laser power density was much more difficult and affected by larger errors.

A brand-new target chamber (diameter of 70 cm) was used, with more input/output flanges (fig. 1 and 2) with respect to the one used in previous experiment [12]. Simple target holder made possible a fast vertical replacement of the irradiated sample and angular rotation of the target. The output windows chosen for diagnostics were the ones placed at angles of 17°, $30^o$, $43^o$ and $56^o$ with regards to the laser beam axis. The system was pumped by a 300 l/s turbomolecular pump to the standard vacuum, below $1 \cdot 10^{-6}$ mbar (registered limit vacuum $7 \cdot 10^{-7}$ mbar).

Three ion collectors (ICs) and cylindrical electrostatic ion energy analyzer (IEA) [13,14] were used for corpuscular diagnostics during experiments. Different types of ion collectors were used:

1) a standard circular flat collector (ICS2, fig. 9) with diaphragm diameter of 0.8 cm.
2) a ring ion collector (ICR) which makes possible the diagnostics of ions emitted close to axis simultaneously with IEA (the smaller diameter is 3.8 cm and the larger one 5.0 cm);
3) an ion collector with suppressed secondary electron emission (ICB1) with a diaphragm diameter of 1.6 cm (deep cup with the cone on the bottom).

Transmission of a grounded mesh in front of the collector is T = 0.58 in all cases. The IEA, which was placed at the window position of 30°, has a bending radius of $R_0$ = 10 cm, the deflection angle is $\psi = 90^o$ and the gap between the cylindrical electrodes of the analyzing capacitor is $\Delta R$ = 1 cm. A windowless electron multiplier (WEM) Thorn EMI EM 226 (fitted with cube dynodes) was used as an ion detector behind the IEA. The path of ion flight was 155 cm for IEA in all experiments, and variable from 43 cm for ICS2 and 50.5 cm for ICB1 to 95 cm for ICR. The sketch of IEA is given in fig. 10.

A $M/\Delta M$ = 200 quadrupole mass analyzer Quadstar 421 was used for the registration of the gas composition in the target chamber during the experiment and of ejected atoms (ions) from the irradiated target [15].

The experimental set-up was the following: a lens with focal length f = 50 cm was used in all the experiments shown in the following. Minimum spot diameter was estimated to be about 0.5 mm at the lens position (L. P.), about 55 cm in front of the target (at 900 mJ pulse energy, the highest attainable laser power density is estimated to be about $5 \cdot 10^{10}$ $W/cm^2$). The measurements also showed large a remarkable change of minimum focal spot either when the laser energy changed and after a few hours.

It is worth mentioning an extreme nonlinearity of the knob position and of the output laser energy.

A measurement of the changes of laser spots was performed by using IR sensitive paper placed at the chamber center for L. P. from 53 cm to 72 cm and for $E_L \sim 310$ mJ. A

minimum focus spot below 0.5 mm was registered at L.P. = 60 cm, but larger spots of 0.6 or 0.7 mm appeared at different laser energy. This problem was settled after the maintenance of the laser and its performance were re-established close to the original ones.

Considering that the target tilt angle was 30°, the ion composition measurements were performed in the direction of the normal to the target. The ion composition of laser plasma produced on Au, Nb, Pb, Ta and W targets was measured at the threshold laser energy $E_L$ ~ 30 to 40 mJ (th) and at maximum available laser energy $E_L$ ~ 300 mJ (hi) for L.P. = 57 cm. The voltage (±U/2) used on IEA varied from a few volts to several hundreds volts, which made possible to register ions with the kinetic energy-to-charge ratio from several tens of eV up to about $E_i$ /q ~ 10 keV.

## 5 THE EXPERIMENTAL RESULTS

Experiments were carried out for different ion species; Nb, Ta, W, Au, Pb ion beams were produced.

Ions up to $Nb^{4+}$ were registered at threshold energies (30 mJ) and up to $Nb^{8+}$ at higher energies (270 mJ). Approximate mean ion velocities <v> and mean ion energies $<E_i>$ calculated from maxima of IC signals were about $2.9 \cdot 10^6$ cm/s and 0.40 keV in the first case, about $4.9 \cdot 10^6$ cm/s and 1.2 keV in the second one. Ion composition of charge–energy distribution for Nb is shown in figs. 11 and 12 for low and high laser energy. Fig. 13 shows the abundancies of different charge states for two laser energies.

Ions up to $Ta^{5+}$ were registered at threshold energies (30 mJ) and up to $Ta^{8+}$ at the highest energies (310 mJ). From the shape of IC signal, two overlapped groups of Ta ions (faster and slower) are visible. Approximate mean ion velocities <v> and mean ion energies $<E_i>$ calculated from maxima of IC signals were about $2.0 \cdot 10^6$ cm/s and 0.40 keV at threshold energies (normal direction), about $3.6 \cdot 10^6$ cm/s and 1.2 keV at highest energies. Fig. 14 shows the abundance of different charge states for two laser energies.

Ions up to $W^{6+}$ were registered at threshold energies (40 mJ) and up to $W^{9+}$ at the highest energies (310 mJ). The shape of IC signals suggests two overlapped groups of W ions (faster and slower) again, but this time it is not so significant. Approximate mean ion velocities <v> and mean ion energies $<E_i>$ calculated from maxima of IC signals were about $2.2 \cdot 10^6$ cm/s and 1.0 keV in the first case (lower energies), and about $4.1 \cdot 10^6$ cm/s and 1.6 keV at higher energies. Figs. 15 and 16 show the W charge-energy distribution for low and high laser energy. Fig. 17 shows the abundancies of different charge states for two laser energies.

Ions up to $Au^{6+}$ were registered at threshold energies (40 mJ) and up to $Au^{10+}$ at higher energies (280 mJ). Two or three groups of ions are remarkable from IC signals for lower and higher $E_L$, one corresponding to impurities, mainly light ions, the other corresponding to Au ions. The same trend was registered with the IEA. The first small peak is composed from both Au ions and impurities (H, C, O), which prevail. From the shape of IC signal two overlapped groups of Au ions (faster and slower) are visible. Approximate mean ion velocities <v> and mean ion energies $<E_i>$ calculated from maxima

of IC signals were about $1.9 \cdot 10^6$ cm/s and 0.37 keV at the threshold energy, and about $3.3 \cdot 10^6$ cm/s and 1.1 keV at the highest energy (both in normal direction). Ion composition of Au laser plasma consists of 55% (50%) of ions with charge state $1^+$ at low (high) laser energy, more than 80% of ions are ions with charges state $1^+$ to $3^+$ (in both cases). With increasing $E_L$ the amount of these ions slightly decreases in the favor of higher charge states. The same behavior was observed for all the ion species. Fig. 18 shows the abundancies of different charge states for two laser energies.

Ions up to $Pb^{4+}$ were registered at threshold energies (40 mJ) and up to $Pb^{9+}$ at higher energies (290 mJ). From the shape of IC signal from all three channels, two overlapped groups of Pb ions (faster and slower) are visible again. Approximate mean ion velocities $\langle v \rangle$ and mean ion energies $\langle E_i \rangle$ calculated from maxima of IC signals were about $1.8 \cdot 10^6$ cm/s and 0.33 keV in the first case, about $2.6 \cdot 10^6$ cm/s and 0.75 keV in the second one.

## 6 ION CURRENT MEASUREMENTS

Maximum ion current density j can be calculated from IC signals:

$$j = \frac{U_{IC\,\max}}{R_l S^* F} \qquad (6)$$

where j is given in mA, $U_{IC\ max}$ is the peak value of IC signal in mV, $R_l$ is the load resistance in Ω, $S^*$ = S x T is the effective surface area of the IC (S = surface of the IC and T = mesh transmission) in $cm^2$ and F = (1+γ/q), being γ the secondary electron emission coefficient. To compare the ion current densities, measured by different ICs at different distances L, it is necessary to recalculate signals by using of $1/L^3$ law.

Ion current densities measured by ICR (perpendicularly to the target) at higher energies were of order of tenths of mA/$cm^2$ for L.P.= 57 cm: the highest values were for Nb ~ 0.7 mA/$cm^2$, for Pb ~ 0.43 mA/$cm^2$, for Ta ~ 0.37 mA/$cm^2$, for Au ~ 0.30 mA/$cm^2$, the lowest being for W (~ 0.15 mA/$cm^2$). Current densities measured by ICB1 and ICS2 should be $(95/50.5)^3 = 6.66$ or $(95/43)^3 = 10.78$ times, respectively, higher. Corresponding values ranged from ~ 2 mA/$cm^2$ (Au, Ta, Pb, W) to ~ 7 mA/$cm^2$ (Nb). Angular distribution of ions is not isotropic; the plume is directed along the normal to the target surface with an angular aperture for heavy metal of about ±20°÷±30°.

In order to optimize the ion production conditions for ECLISSE project demands, we measured IC signals by changing the lens position with regard to the target (Ta, $E_L$ ~ 270 mJ). While the ion current density j at L.P.= 57 cm was about 0.35 mA/$cm^2$ (at the distance of 95 cm), it increased ~ 3 times for L.P.= 60 cm. Recalculating this value of 1 mA/$cm^2$ to the distance of 20 cm from the target ($(95/20)^3$ ~ 107) we obtain the current density j ~ 100 mA/$cm^2$.

Considering that the extraction aperture will be about 3 $cm^2$, a total current of about 1 A or higher can be injected into the ECR plasma during a few tens μs. The mean ion energy $\langle E_i \rangle$ was ~ 1.2 keV in the first case and it decreased to ~ 600 eV in the second one. Ions with charge states up to 8+ were registered, but those with 1+ and 2+ prevail. As above stated, such results are not critical for the ECLISSE project because the final CSD

slightly changes if ions are injected with charge state 2 or 10. The highest current density (about 2.2 mA/cm$^2$ at the distance 95 cm) was measured at L.P = 66 cm, but $<E_i>$ increased to 1.6 keV in this case. Thus the increase of current density will be not effective because the coupling efficiency will be lower. These results are comparable with the previous ones, which were performed with different experimental conditions [12]. In that case the ion current densities around j ~ 80 mA/cm$^2$, recalculated to the distance 20 cm, were obtained for Ta, j ~ 100 mA/cm$^2$ for Ni and j ~ 120 mA/cm$^2$ for Al at $E_L$ ~ 300 mJ and L.P. = 55cm. Ion current densities (recalculated again to 20 cm) of j ~ 300- 400 mA/cm$^2$ for Cu target were obtained at L.P. 57-60 cm, and j ~ 160 mA/cm$^2$ at L.P. 65 cm (at $E_L$ ~ 370 mJ).

In conclusion, the amount of LIS-produced ions is in good agreement with our expectation; anyway it must be taken into account that it depends not only on the laser power density, deposited on the target, but also on the volume of the produced plasma (diameter of the laser focus spot). It reflects very sensitively all changes of laser caustics with regard to the target surface position, caused either by the change of lens position, or by the change of laser divergence (in dependence on the laser energy, as experimentally demonstrated also in [12]). In addition, analogous dependence of the mean ion energy $<E_i>$ on the laser pulse energy $E_L$ is obtained.

Such sensitivity may be a major obstacle to a stable injection of the LIS beam to the ECRIS and finally to the ECRIS output.

## 7 COMMENTS

Ions with maximum charge state $8^+$ to $10^+$ were detected among those emitted from the Nd:YAG laser produced plasma of different elements (Nb, Ta, W, Au, Pb) at laser power densities ~ $10^{10}$ W/cm$^2$. More than 70 % of ions have charge states lower than $4^+$ for all tested elements and in any condition. The ion current density at the distance of 20 cm from the target depends on the kind of target, as well as on the experimental conditions (laser energy, spot diameter, laser power density, target surface). Its value is above ~ 100 mA/cm$^2$, higher for lower-Z elements and lower for high-Z elements. The mean velocity of ions, emitted perpendicularly to the target at energies ~ 300 mJ, ranged from $2.6 \cdot 10^6$ cm/s (Pb) to $4.9 \cdot 10^6$cm/s (Nb), corresponding to mean ion energies from ~ 750 eV (Pb) to 1.2 keV (Nb). Angular distribution of emitted ions is not isotropic [16].

Generally, three ion groups (thermal, fast, slow), besides that of impurities, may be emitted from the laser produced plasma [17,18]. The main one corresponds to the thermal ions, the second (”slow”) one appears due to reabsorbed x-rays outside the laser focus, the third one (”fast”) is ascribed to the presence of suprathermal (hot) electrons. The IC signals, in dependence on the laser power density, may overlap each other and create several more or less pronounced maxima, the position of which and their amplitude may reflect not only mechanism of ion production, but also variations of laser parameters or quality of its beam (the shape of laser pulse, prepulses, changes of the laser energy, radial inhomogeneity, hot spots etc.) [19]. The higher is the laser power density, the higher is the ion energy and charge state of produced ions. The highest power density supposes the

smallest size of the focal spot at a given laser power, which, in turn, does not mean that the highest number of ions are produced.

This is due to the nonlinear effect of laser beam focus position on ion generation [20]. Depending on the laser power density, it is possible to generate a smaller amount of higher energy ions or a larger amount of low energy ions.

The possibility to 'tune' the laser ion source in order to optimize the further ionization by means of the ECR plasma was fully demonstrated; the ion current and the ion density are coherent with the theoretical assumptions described in §2 and §3, which leaves us confident in the success of the hybrid ion source.

## 8 THE EXPERIMENTAL SET-UP AT IPPLM

Experiments have been carried out at IPPLM in Warsaw in order to show the beneficial effects of a magnetic axial field and of a bias voltage on the extraction of the ions from the laser-produced plasma.

The investigations on the influence of external magnetic and electric fields on the characteristics of tungsten ion stream emitted from a laser produced plasma were performed with a Nd:glass laser. A negatively biased target up to –15 kV and a magnetic field up to 0.45 T were used in the experiment. A set of ion collectors and an electrostatic cylindrical ion energy analyzer located at small angles with respect to the laser beam axis and at large distances from the target were applied for ion measurements (fig. 3).

The ion collectors consist of 17 Faraday cups biased negatively (-40 V) and they were arranged along two perpendicular directions: 5 collectors placed in north (5 collectors), south (5 collectors) and west (S1-S5 collectors) directions and 2 collectors in east direction. S1-S5 collectors are located at distances about 78.1 cm from the target at angles of 2.1°, 3.2°, 4.3°, 5.4° and 6.5° to the target normal. The effective aperture area of each collector is 0.114 $cm^2$ (solid angle of measurement of $1.867\times10^{-5}$ sr).

The IEA was located at 6° to the target normal and 181.8 cm from the target. A windowless electron multiplier was used as a detector at the output of the IEA. The pressure inside the target chamber and the IEA was in the range of $10^{-6}$ Torr, about one order of magnitude worse than in the experimental setup at LNS. This difference may partially explain the smaller percentage of high charge states in the spectrum, because of recombination phenomena in front of the target. The ion diagnostics for measuring ion stream parameters, i.e. a set of ion collector and an electrostatic cylindrical ion energy analyzer, IEA (fig. 10), were based on the time-of-flight method [13].

The laser beam ($E_L \leq 1.5$ J, $\tau_L \sim 1$ ns, $\lambda_L = 1.06$ μm, laser beam diameter of about 20 mm, laser beam divergence of 0.5 mrad) was focused normally to the target surface by means of a lens with the focal length of f = 133.4 cm (large focal length will be used for the real ion injector of the hybrid ion source) onto thick W disc targets of purity above 99.0%. The target was polished and cleaned before putting it inside the target chamber. It was fastened to the target holder placed 0.8 cm out of the laser beam axis to assure manifold laser shots on fresh target surface. The target holder construction makes it

possible to bias the target $U_t$ to a high voltage ranging from +10 kV to -15 kV and to produce a symmetric electric field in the space limited by the grounded shielding tube, the target and the grounded diaphragm. This space is also filled by nearly symmetric uniform longitudinal magnetic field with induction of $B$ = 0.45 T generated by Helmholtz coils. The coil pulse is in coincidence with the laser shot, so that the magnetic field is constant before and after the ion pulse duration.

The lens was placed outside the target chamber and could be moved for focusing within the range from –1.5 cm to +10 cm. The focus position, FP was changed over the range from –1.5 cm to +10 cm (FP = 0 means that the target is located in the focus point, signs "-" and "+" mean that the focus point is in front of the target surface and inside the target, respectively).

## 9 EXPERIMENTAL RESULTS AT IPPLM WITH FREELY EXPANDING PLASMA

Ion collector signals measured for the 1$^{st}$ laser shot show the existence of a large amount of contaminant ions and a small amount of W ions, and it should be treated as a laser cleaning shot (fig. 19). For comparison fig. 20 shows the S1-S4 signals for the 2$^{nd}$ laser shot. It is seen from this figure that the amount of contaminant ions (on the left of the curves) is much lower than in fig. 19 while the amount of W ions for the 2$^{nd}$ laser shot is not so different. Fig. 21 shows the comparison of ion spectra measured with the use of the IEA for the 1$^{st}$ laser shot onto the fresh W target surface and for the 2$^{nd}$ laser shot onto the same place on the target surface as the 1$^{st}$ laser shot.

On the basis of a series of IEA spectra measured at different analyzing potentials at nearly the same experimental conditions we reconstructed the S4 collector signal (fig. 22). Since the gain of the WEM was not taken into account the reconstructed S4 signal gives only qualitative information on the abundance of ion species. However, it gives information on the ranges of time of flight (or velocity, or energy) of ions in detail. It is seen that the valley on the collector signal, between the faster and slower groups of ions, practically separates the signal of contaminants and the signal of tungsten ions, especially interesting for us. The faster ion group of the collector signal contains mostly ions of light contaminants (mainly $H^+$, $C^+$, $O^+$, $C^{2+}$, and $O^{2+}$). The slower ion group contains W ions only.

A series of laser shots was performed to investigate the effect of the influence of focus position on W plasma expansion. The focus position was changed over the range from -1.5 cm to +10 cm. The charge carried by W ions $Q_i$[C/sr], the average ion kinetic energy $\langle E_i \rangle$[keV], the maximum ion current density $j_{max}$[mA/cm$^2$] and the maximum recorded charge state $z_{max}$ of W ions obtained for the 2$^{nd}$ laser shot onto the target were measured as a function of focus position.

$Q_i$ and $j_{max}$ have minima, $z_{max}$ has maximum at specific value of FP = +4 cm while the $\langle E_i \rangle$ is nearly constant for FP from 0 to 10 cm as shown in fig. 23. There is a focus

position between 0 and +2 cm which optimises $z_{max}$ and $j_{max}$ with a low $<E_i>$ at the same time.

The dependence of the charge carried by W ions, $Q_i$ (a), the average ion kinetic energy, $<E_i>$ (b) and the maximum ion current density, $j_{max}$ (c), on the laser energy $E_L$ were measured by the S1 collector in two runs, as shown in fig. 24. The laser energy ranged from 0.25 to 1.2 J at a given focus position FP = +10 cm. The scaling of these parameters as a function of the laser energy differs slightly for the presented two runs. It is remarkable that the ion energy scales linearly with the laser energy in this regime.

Multiple laser shots onto the same place of the target surface were also tested and the results obtained (relative to the FP = -1.5 cm) have shown that the charge carried by W ion group and the ion current density with exception of the 1st laser shot (cleaning shot) are practically independent over the 12 successive laser shots. The average ion energy slowly increases with the number of laser shots and for the 13th shot is 1.5 times higher that for the 2nd shot. It was observed that a number of successive laser shots onto the target under our experimental conditions does not essentially change the ion collector signal parameters with exception of the 1st laser shot onto fresh target surface

On the basis of ion collector measurements the ion velocity distributions for S1- S4 collectors placed at different angles with respect to the target normal, in the range from 2° to 6°, were calculated. In the case of freely expanding plasma the highest maximum velocity of ions is observed for S1 collector. For S2−S4 collectors the maximum velocities have nearly the same values. The velocity distributions for S1 and S4 differ slightly in amplitude with a factor of about 2. Fig. 25 shows an example of the ion velocity distributions for freely expanding plasma calculated on the basis of S1-S4 collector signals for three laser energies (0.45, 0.52 and 1.11 J).

## 10 THE INFLUENCE OF MAGNETIC AND ELECTRIC FIELDS ON THE PLASMA EXPANSION

The expansion of laser-produced plasma in external magnetic field was measured for B = 0.45 T and FP = +10 cm. Amplitudes of the W ion group signals recorded with the use of ion collectors are several times higher than for B = 0 case. The amplitudes of signals containing mainly contaminants are similar in both cases.

The ion velocity distributions of W plasma expanding in presence of magnetic and electric fields as compared to the case of freely expanding plasma, shown in fig. 26 (S1-S4 collector signals). The distributions for B = 0 and U = 0 significantly differs from the ones obtained for B = 0, $U_t$ = -5 kV, and B= 0.45 T, $U_t$ = 0. The application of $U_t$ = -5 kV results in the decrease of the maximum velocity of ions from the original value of (4.5-5) $\bullet 10^7$ cm/s to about $2\bullet 10^7$ cm/s. The amplitudes of the ion velocity distributions of W ion with ion velocities of about $2.5\bullet 10^6$ cm/s for the B = 0, $U_t$ = -5 kV case are about 5 times lower in comparison with the case B = 0.45 T, $U_t$ = 0; the amplitudes for B = 0, $U_t$ = 0 and B = 0, $U_t$ = -5 kV are similar in that range, whereas many more fast ions are present in the case B

= 0, $U_t$ = 0. Fig. 27 shows a partial view of the distribution corresponding to a velocity below $2 \cdot 10^7$ cm/s.

Unfortunately the decrease of the ion energy with the negative bias was not always reproducible; in fact, potentials generated on the externally supplied target had a bipolar structure reaching values up to $V_t$ = |30| kV and recorded for about 200 ns after the laser pulse (fig. 28). Probably, owing to this bipolar potential, the ions cannot be effectively decelerated in the external electric field. This phenomenon was observed for different laser energy (0.33 and 0.75 J in fig. 28).

In conclusion, from the tests performed at IPPLM, we have obtained the following information [6]:

- Ion collectors signals have two-peak structure, the first peak (the faster group) contains mainly contaminant ions, the 2nd peak (the slow group) contains mainly low charged W ions.
- The parameters of ion collector signals remain similar during at least 10 (successive) laser shots to the same place on the target excluding the 1st laser shot.
- Ion collector signals and the IEA spectra for 1st laser shot show the existence of large amount of contaminants (mainly H, C and O ions). This emission can originate some problems for ECLISSE experiments because of space charge effects.
- Strong defocusing of the laser beam (FP = 10 cm in our experimental conditions) provides a large current of slowly charged W ions at least for twelve successive laser shots.
- The effect of the plasma stream compression due to external longitudinal magnetic is evident.
- The plasma cannot be effectively accelerated or decelerated, because of the bipolar potential created on the target during the laser pulse. The most probable reason of the 25 kV positive signal is a strong electron emission in the early stage of laser-plasma interaction. This shielding mechanism will be investigated.
- Values of the parameters, which are important for the coupling of the LIS to the ECR, were estimated for the freely expanding laser-produced plasma as it follows: $\langle E_i \rangle \sim$ 0.5-2 keV, i.e. 0.2 to 0.7 keV per charge state, $j_{max} > \sim$ 1-8 mA/cm$^2$ (at the distance of 78 cm from the target, or 60-480 mA/cm$^2$ recalculated to the distance of 20 cm) in dependence on the $E_L$ and FP, in good agreement with the results obtained at LNS.
- Some precautions must be made (an adequate distance between the focusing lens and the entrance glass window on the experimental chamber) to prevent this window against destruction due to too high laser energy density on the window.
- The laser produced-plasma expansion in the external electric field is also influenced by a plasma effect in the space in which the plasma is separated into electron and ion components. It means that a simple assumption on electrostatic deceleration of ions in a vacuum cannot be realized experimentally in our case. For future experiments we are preparing another electric system for removing contaminant ions and selecting the ions with energy appropriate for efficient coupling of the LIS to the ECRIS.

## 11 STUDY OF THE ETCHING RATES

The laser interaction with metallic surface produces a high etching for a pulse energy higher than a threshold value typical of each metal. Near the threshold a strong neutral emission takes place and then also a stronger ionic emission occurs. At LNS we have demonstrated that the experimental thresholds for the ion emission is very similar to the threshold for the neutral emission. The atomic neutral emission was monitored by a mass quadrupole spectrometer and by the vapor thin film deposition technique. The energy thresholds, the emission yields, the angular distribution, the fractional ionization, the kinetics and characteristics of the plasma production and the ion charge state have been studied for Al, Ti, Ni, Cu, Nb, Sn, Ta, W, Au and Pb targets [21,22,23].

A mass quadrupole analyzer (MQS), 1-210 amu detection range, is located 100 cm from the target with $2 \cdot 10^{-4}$ sr detection solid angle. It was employed to detect the neutral atomic component ejected from the target. The MQS was placed at -30° angle with respect to the laser beam direction.

The angular distribution of ejected species from the irradiated target was investigated for the ion component using the ion collectors and for the total (ionic and neutral) component by measuring the thin film thickness deposited on carbon substrates placed around the target. This last measurement was performed with a scanning electron microscope (SEM) using 30 keV electron microprobe to induce the characteristic X-ray fluorescence emitted from the deposited film, as presented in a previous paper [24].

The metal etching occurs only above a given threshold, which is high for elements with high binding energy, as reported in our previously paper [25]. Typical examples of results obtained for two different metals, aluminum and gold, respectively with a binding energy of the molecules about 1.38 and 2.34 eV, are presented in Fig. 29. This figure shows the experimental energy threshold measured for neutral (a) and for ionic (b) components as a function of the laser fluence.

The laser fluence thresholds for the neutral emission are 5.0 and 15.0 J/cm$^2$ for Al and Au, respectively (fig. 29a). At this laser wavelength, assuming a reflectivity of 0.97 for Al and 0.99 for Au, according to the literature [26], this means a threshold for the absorbed energy density ($E_{thrs}^{0}$) corresponding to 0.15 J/cm$^2$ both for Al and Au.

The experimental laser fluence thresholds for the ion emission are 4.6 and 16.0 J/cm$^2$ for Al and Au, respectively (fig. 29b). The reflectivity indicates an absorbed ion energy threshold ($E_{thrs}^{n+}$) corresponding to 0.14 and 0.16 J/cm$^2$ for Al and Au, respectively.

This comparison indicates that each metal has a typical threshold for the laser etching process and that this threshold value is about the same both for neutral and for ion emission.

In other words, results obtained at 1064 nm wavelength, indicate that the laser etching originates the emission of neutrals and ions at the same laser fluence. Literature reports that using UV laser radiation (for which the reflectivity and the penetration depth is

lower) the threshold for the ion emission is higher than that for the neutral emission, as reported in ref. [27].

Table 4 reports a comparison between the theoretical and the measured energy density thresholds for the neutral and ion production for many metals. The experimental data show an agreement between neutral and ion thresholds, except for Ta and Pb; in these cases the agreement is not so good, probably because the assumed metal reflectivity value is not correct. The reflectivity coefficient, in facts, depends on the metal temperature, on the solid-liquid phase, on the incident angle and on the presence of a plasma region formed in front of the target surface. Thus, in many cases the reflectivity value cannot be exactly evaluated.

The energy density threshold measurements are in good agreement with the theoretical previsions given by a classical thermal model, except for Sn and W. It is assumed that the threshold corresponds, approximately, to the minimum energy density, $E_o$, needed to evaporate the irradiated mass into vacuum [25].

In order to measure the neutral and ionic emissions, two different experimental approaches have been used.

The first approach was based on the mass loss of the irradiated target due to a known number of laser pulses. This measurement gives an indication about the total emission (neutral and ionic). The etching yield, Y, was measured in terms of ejected atoms per pulse. Near the threshold the experimental number of ejected atoms is in agreement with the atom number of the irradiated mass, *m*, calculated using the quantity $m = \rho S \delta$, where $\rho$ is the target density, S the laser spot surface, $\delta$ the absorption depth,

Generally, the etching yield increases linearly with the pulse energy. Sometimes, at very high fluences, it increases almost exponentially, as results of the non-equilibrium “splashing effect”, characterized by clusters and micron-sized granular emission emitted with the atomic component [28].

The second approach is referred to the ion emission from the irradiated target. An ion

collector measures the ion current vs. time. The collector, consisting of a Faraday cup using an input grid as secondary electron suppressor, measures the ion current vs. time. The ion charge distribution, Q(t), can be calculated from the formula [13]:

$$\frac{dQ}{dt} = \frac{V_C(t)}{T \cdot R \cdot F(t)} \qquad (7)$$

where $V_c$ is the voltage amplitude of the collector signal (mV), T is the transmission of the IC entrance grid (58 %), R is the load resistance (25 Ω) and F(t) is a function depending on the secondary ion electron emission coefficient and on the ion charge state, which, in our experimental conditions, is about $F(t) \sim 2$.

Near the threshold the average ion current is low. Generally it increases approximately linearly with the laser pulse; the average voltage, $V_c$, can be converted as average number of ions per pulse.

The angular distributions, both for the total emission and for the ionic emission, have been obtained by the thickness measurement of thin films growth on carbon substrate and by the IC detector placed at different angles around the target, respectively.

Although deposited atoms produce sputtering effects, which can modify the deposited film thickness, at this stage we have preferred to report experimental data without any correction. The presented data for neutral emission can be underestimated, because the sputtering yield depends on the incidence angle as $(\cos\theta)^{-1}$, where $\theta$ is the incident angle and then the sputtering effect may produce a most peaked angular distribution of the total emission, especially for heavy atoms.

A work is in progress to improve experimental results measuring the corrective factors for the sputtering effects on the total emission.

Without sputtering corrections, results indicate that for each target both neutral and ion angular distribution are very similar. However, different angular distributions are found for different targets. Fig. 30 shows a comparison between Cu and Pb distributions (the metal targets are irradiated under the same experimental conditions, at a laser pulse energy $E_L$ = 875 mJ). According to the literature, low-Z metals have a broader distribution with respect to the heavier elements [24] whereas the ion distribution measurements, performed by our group has given controversial results [16].

Tab. 4 shows the calculated reflectivity for different metal targets, the experimental energy density threshold for neutrals ($E_{thrs}{}^{0}$) and for ions ($E_{thrs}{}^{n+}$) and the theoretical energy density threshold for neutrals ($E_o$); moreover, in the table the solid angle covered by the total emission, $\Delta\Omega_T$, for different targets, calculated as FWTM (full width tenth maximum) of the angular distribution, is given. In order to compare the total emission $N_t$ with the ionic one $N_i{}^{q+}$, the number of ions detected by IC was multiplied by the factor $W_f=\Delta\Omega_T/\Delta\Omega_{IC}$. The factors $W_f$, used for each element, are reported in Tab. 4.

For gold, as an example, at a laser fluence just above the threshold (15 J/cm$^2$), we find $6\bullet10^{14}$ as total number of particles (neutral and ions) emitted per pulse. The number of detected ions is $4\bullet10^{10}$/pulse, corresponding to a total ion emission of $6.2\bullet10^{13}$ ions/pulse, after the $W_f$ factor correction. The Au total emission rises to $3.4\bullet10^{15}$ at a laser fluence of 150 J/cm$^2$.

High fractional ionizations are obtained for metals having low binding energy and low melting points [15].

For increasing laser fluence, both the neutral and ionic components increase, and generally, the fractional ionization increases, too.

Tables 5 and 6 report the comparison of the fractional ionization ($N_i{}^{1+}/N_t$) for different metals irradiated both near the threshold (low fluence) and at a fluence about ten times the threshold value (high fluence). It is possible to observe that, at low fluence, the fractional ionization ranges between 3 % for Ni up to 40 % for Pb, while, at high fluence, it ranges between 20 % for Ni and Ta up to 52 % for Al. Some data are lacking in Table 6 and further measurements are in progress. Generally, in order to have a fractional ionization higher than 50 %, very high laser fluences are needed.

In conclusion, the original result obtained in the frame of the ECLISSE experiment was the observation that the thresholds for the emission of ions and neutrals are so similar at 1064 nm. Because the plasma plume at the threshold is too weak to absorb IR laser light, probably this result derives by the mechanism of energy absorption by the free electrons in the metal. Electrons absorb the energy by multi-photons processes and by electron-electron interactions and reach energies so high to induce ionization by electron-ion impact. At higher fluence the plume absorbs the IR laser and the ionization increases, because of warm plasma formation on the target surface.

## 12 COMPARISON OF IONIC CURRENTS AND ETCHING RATES

From the point of view of the coupling of the Laser Ion Source (LIS) to ECRIS, LIS-produced ions can be used only if their energy is of the order of hundreds eV, i.e., sufficiently low to permit the trapping and the further ionization in the plasma region of ECR ion source [1,2,4]. Preliminary measurements performed with IEA indicate that near the threshold, although the main ionic component has a low charge state (1 - 3), a low energy distribution occurs, with an average value around 100-300 eV. These conditions are favorable for injection of these ions in the ECRIS.

In order to give a first evaluation of the ion current extractable from the LIS, we must consider the yield of ion production per pulse. Thus, for many elements, at a target distance of 51 cm, we have measured a yield of the order of 1 to $5 \cdot 10^{12}$ ions/pulse/cm$^2$ with the maximum flux directed along the normal to the target surface. Supposing that the most of ions have a single or double charge state and working with 30 Hz repetition rate, it is possible to extrapolate a number of particles around $10^{14}$ pps/cm$^2$, i.e. an average current of the order of 15 pμA/cm$^2$. However, if the strong magnetic field of SERSE will permit to focalize and to inject all ions ejected from the irradiated target into the plasma, it could be possible to increase this quantity even by one order of magnitude.

## 13 THE ASSEMBLY OF THE HYBRID SOURCE

The assembly of the hybrid ion source will be carried out in 2002 according to the scheme presented in fig. 32 and 33. The support of the Nd:YAg laser is ready and the installation in the ECRIS area will be carried out during a period of maintenance of the ECR ion sources.

In fig. 34 a cross section of the SERSE plasma chamber is shown with the metal target placed on a rotating rod in the injection side of the chamber. A displacement system has been prepared and tested to irradiate a sample on a fresh surface following an annular shape of the irradiated area (30 minutes, 30 Hz for the Aluminum sample in fig. 35).

Because of the cryostat, there is no radial accessibility to the plasma chamber of SERSE and even the axial accessibility is poor because of the extraction system on the left side and the biased electrode, the microwave and gas inputs on the right side. Therefore the easier solution is to inject the laser beam from the extraction hole, because laser optics cannot be used inside the ECR plasma chamber. The laser beam will be injected from the

0° port of the 90° analysis magnet (fig. 32), on-axis with the extracted beam (the interaction between the laser beam and the beam of highly charged ions extracted from the source is negligible).

In fig. 34 a lateral view of the experimental setup is also shown. The 8 mm hole of the extraction system (located 250 mm inside the cryostat, on right side in fig. 34) will be increased to 12 mm to prevent any damage to the extractor because of the erosion caused by the halo of the laser beam. The sketch in fig. 34 shows the target in the plasma chamber. It will be located in place of the existing negatively biased electrode.

A removable shield, cylindrically shaped, will be used inside the chamber to collect the cluster emission from the target. It will be changed periodically to maintain the plasma chamber clean, which is mandatory for a good production of high charge states ion beams (charge exchange processes can reduce substantially the yield of the highest charge states). We expect to pump the target holder chamber with the same turbomolecular pump which is used now for the injection side of SERSE, in order to reach a vacuum in the order of a few $10^{-8}$ mbar.

The Nd:YAg laser will be aligned onto the target, by means of a He-Ne laser, and a focusing lens will be placed at about 20 cm from the 0° flange of the magnet, in order to have a beam spot dimension variable from 1 to 8 mm at the target position. The Nd:YAg laser will be operated at some hundreds mJ up to the maximum energy, with a repetition rate of 30 Hz or lower, in order to produce a plasma on the target surface.

In order to simulate the effective lens-to-target distance (4 m) the plasma chamber has been moved 350 cm far from the previous position and the tests in this setup are now under way. After some tests devoted to get some experience with this setup, the laser will be moved for the hybrid source tests.

## 14 CONCLUSIONS

The relevant number of tests which have been carried out in the frame of the ECLISSE project have demonstrated that the solution of the hybrid ion source is viable and that important improvements can be obtained in the field of ion sources by coupling two powerful types of sources as LIS and ECRIS.

Further tests will be carried out in terms of stability and reproducibility in the coming months (these parameters are particularly delicate for a LIS and tests up to 30 minutes have demonstrated a stability in the order of 10%, good enough for our purpose). Anyway we believe that the study is mature for the last phase, consisting of the insertion of the LIS target inside the SERSE plasma chamber, as described in §13.

In addition, the perspective which can be opened by the new generation of ECRIS as the gyroSERSE source [31] is attractive, because their larger plasma length and higher plasma density will make less critical the limits on some parameters of the LIS and about one order of magnitude higher energy will be allowed, as demonstrated in §2. Moreover the larger plasma energy content $n_e kT_e$ will be much higher and higher beam currents injected by the LIS may be tolerated by the plasma.

## 15 ACKNOWLEDGEMENTS

This work was supported by the Fifth Committee of INFN and partially supported by the grant A 1010105 from the Grant Agency of the Academy of Sciences of the Czech Republic.

Studies performed at the IPPLM in Warsaw are partially supported by the Polish State Committee for Scientific Research within the KBN grant No. 5 P03B 108 20.

The support of S. Marletta, F. Chines, E. Messina, C. Percolla is gratefully acknowledged.

## 16 REFERENCES

(1) S. Gammino, G. Ciavola, L. Torrisi, L. Celona, Study of charge state enhancement by means of the coupling of a Laser Ion Source to the ECR ion source SERSE, Proc. of the 14th Workshop on ECR ion sources, Geneve, (1999), 98 ECRIS workshop, Geneva (1999)

(2) S. Gammino, G. Ciavola, L. Torrisi, L. Celona, J. Wolowski, E. Woryna, P. Parys, L.Laska, J. Krasa, G.D. Shirkov, Preliminary tests for the electron cyclotron resonance ion source coupled to to a laser ion source for charge state enhancement experiment, Rev. Sci. Instr. 71(2), (2000), 1119

(3) S. Gammino, L. Torrisi, L. Andò, G. Ciavola, L. Celona, L. Laska, J. Krasa, M. Pfeifer, K. Rohlena, E. Woryna, J. Wolowski, P. Paris, G.D. Shirkov. Production of low energy, high intensity metal ion beams by means of a Laser Ion Sources, Rev. Sci. Instr. 73 (2), (2002), 650

(4) L. Andò, L. Torrisi, S. Gammino, G. Ciavola, L. Celona, L. Laska, J. Krasa, J. Wolowski, E. Woryna, G. D. Shirkov, Slow ion beams from a laser ion source for the ECLISSE experiment, It. Phys. Soc., Conf. Proc. PIBHI 2000, SIF V. 72, S. Gammino and G. Ciavola Eds., Bologna (2001), 109

(5) J. Wolowski, L. Celona, G. Ciavola, S. Gammino, J. Krása, L. Láska, P. Parys, K. Rohlena, L. Torrisi, E. Woryna, Expansion of tungsten ions emitted from laser-produced plasma in axial magnetic and electric field, Laser and Particle Beams, to be published

(6) E. Woryna, P. Parys, J. Wolowski, L. Celona, G. Ciavola, S. Gammino, L. Torrisi, J. Krása, L. Láska, K. Rohlena, Influence of external magnetic and electric field on properties of an ion beam emitted from laser-produced plasma, Proc. of SPIE vol 4424 (26th Eur. Conf.on Laser Interaction with Matter, Prague), ed. M. Kalal, K. Rohlena, M. Sinor (2001) 476

(7) G.Shirkov, Different modes of laser ion loading into ECR ion source, preprint RIKEN, RIKEN-AF-AC-28 (2001) 20

(8) G.Shirkov, Simulation of Laser ion loading into ECR ion source, Rev. of Sc. Instrum. 73 (2), (2002), 647.

(9) Shirkov G., Plasma Sources Sci. Technol. 2, 250, (1993).

(10) Shirkov G., CERN Report, CERN/PS 94-33 (HI), (1994).

(11) G.D. Shirkov, S. Gammino, G. Ciavola, L. Celona, Ion loading into ECR source, Physica Scripta T92 (2001) 214

(12) Láska L., Krása J., Gammino S., Ciavola G., Torrisi L., Andó L., Celona L., Marletta S., Messina E., Report INFN-LNS 18-04-00, (2000).

(13) Woryna E., Parys P., Wolowski J., Mróz W., Laser Part. Beams 14 (1996) 293.
(14) Láska L., Krása J., Masek K., Pfeifer M., Králiková B., Mocek T., Skála J., Straka P., Trenda P., Rohlena K., Woryna E., Farny J., Parys P., Wolowski J., Mróz W., Shumshurov A., Sharkov B., Collier J., Langbein K., Haseroth H., Czech. J. Phys. 46 (1996) 1099.
(15) L. Torrisi, L. Andò, S. Gammino, J. Krasa and L. Laska, Ion and neutral emission from pulsed laser irradiation of metals, Nucl. Instr. and Meth. B 184, (2001) 327
(16) L. Laska, J. Krasa, M. Pfeifer, K. Rohlena, S. Gammino, L. Torrisi, L. Andò, G. Ciavola, Angular distribution of ions emitted from Nd:YAG laser-produced plasma, Rev. Sci. Instr. 73 (2), 2002, 654.
(17) J. Wolowski et al., 12 th Int. Conf. LIRPP, Osaka, 1995, AIP Conference proceedings 369 (Eds. S. Nakai, G.H. Miley), Woodbury, New York, Part 2, 1029.
(18) K. Rohlena et al., Laser Part. Beams 14 (1996) 335.
(19) Láska L., Krása J., Masek K., Pfeifer M., Rohlena K., Králiková B., Skála J., Woryna E., Parys P., Wolowski J., Mróz W., Sharkov B., Haseroth H., Rev. Sci. Instrum. 71 (2000) 927-930.
(20) J. Krása et al.: Proc. XXIV. ICPIG, Warsaw, 1999, (Eds. P. Pisarczyk et al.), Vol. II., p. 103.
(21) L. Torrisi, S. Gammino, G. Ciavola, L. Andò, L. Làska, J. Kràsa and M. Pfeifer “Plasma production by laser ion source at the INFN-LNS of Catania”, Report Laboratori Nazionali del Sud, INFN-LNS, in press, 2001
(22) L. Torrisi, S. Gammino, G. Ciavola and L. Andò, “Ion production by pulsed laser beam”, Rep. INFN-LNS Activity 96-99, 233-236, INFN Publ. 2000
(23) L. Torrisi, L. Andò, S. Gammino, G. Ciavola, L. Celona, S. Genovese, L. Laska and J. Krasa, “Intense flow of neutral and ions from laser ablation of metals”, It. Phys. Soc., Conf. Proc. PIBHI 2000, SIF V.72, S. Gammino and G. Ciavola Eds., Bologna (2001), 115
(24) L. Torrisi, L. Andò, S. Gammino, G. Ciavola and A. Barnà, “Angular distribution of ejected atoms from Nd:Yag laser irradiating metals”, Rev. Sci. Instr., 72(1),(2001),68
(25) L. Torrisi, G. Ciavola, S. Gammino, L. Andò, A. Barnà, L. Laska and J. Krasa, “Metallic etching by high power Nd:Yag pulsed laser irradiation”, Rev. Sci. Instr. 71(11), (2000), 4330.
(26) CRC, Handbook of Chemistry and Ohysics, 75th ed., edited by D.R. Lide, Chemical Rubber, Boca raton, FL, 1995
(27) L. Torrisi, S. Trusso, G. Di Marco and P. Parisi, “Pulsed laser deposition of Hydroxyapatite films by KrF excimer”, Physica Medica XVII(4), (2001), 227
(28) P. Baeri, L. Torrisi, N. Marino and G. Foti, "Ablation of hydroxyapatite by pulsed laser irradiation", Appl. Surf. Sci. 54, (1992), 210
(29) S. Gammino, G. Ciavola, L. Celona, The GyroSERSE project, It. Phys. Soc., Conf. Proc. PIBHI 2000, SIF V.72, S. Gammino and G. Ciavola Eds., Bologna (2001), 157

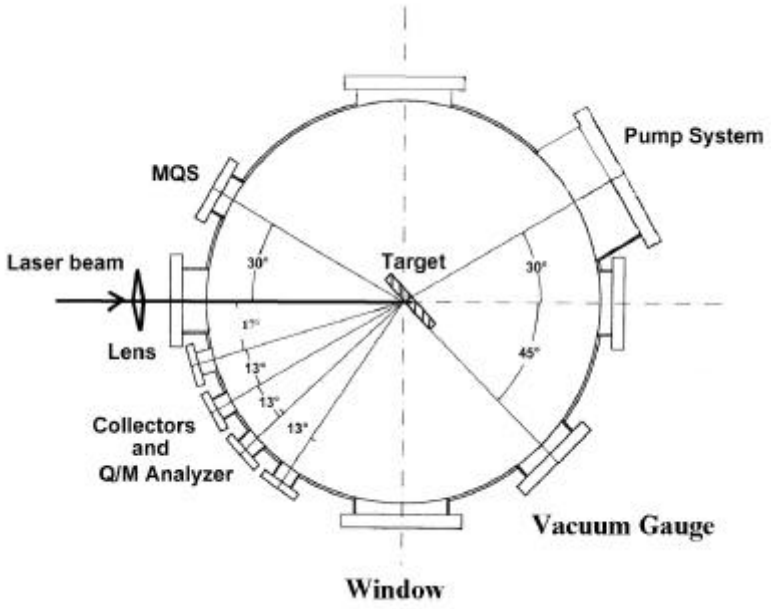


**Fig. 1** – The scheme of the ECLISSE chamber at LNS.

**Fig. 2** – A view of the ECLISSE facility at LNS.

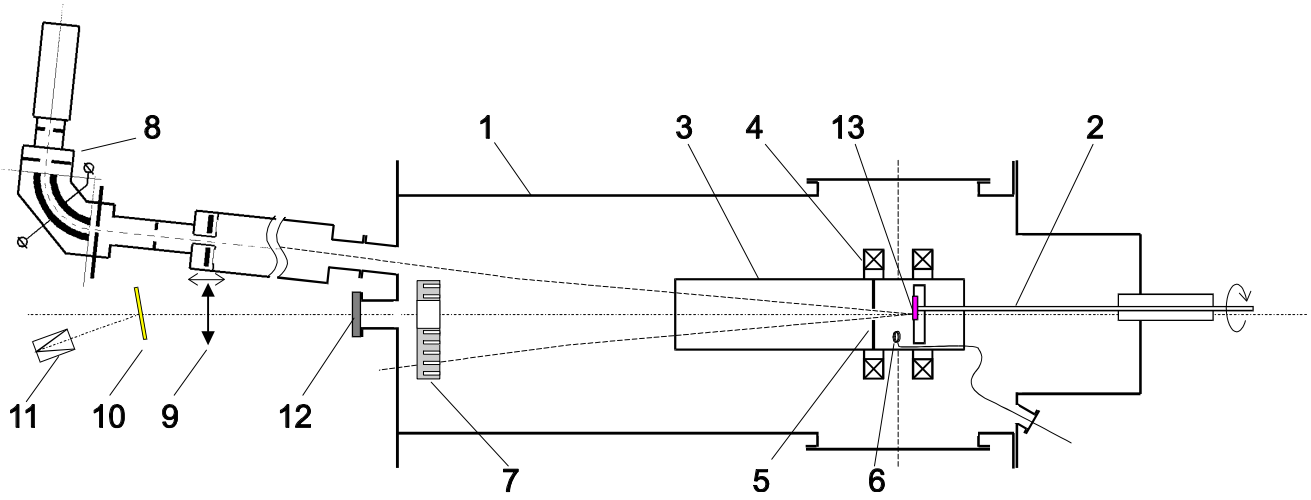


**Fig. 3.** Scheme of experimental set-up at IPPLM: 1 – target chamber, 2 – target holder, 3 – shielding tube, 4 – Helmholtz coils, 5 – grounded diaphragm, 6 – magnetic probe, 7 – set of ion collectors (SIC), 8 – electrostatic ion energy analyzer (IEA), 9 – focusing lens, 10 – splitter, 11 – laser energy meter, 12 – glass window, 13 – target.

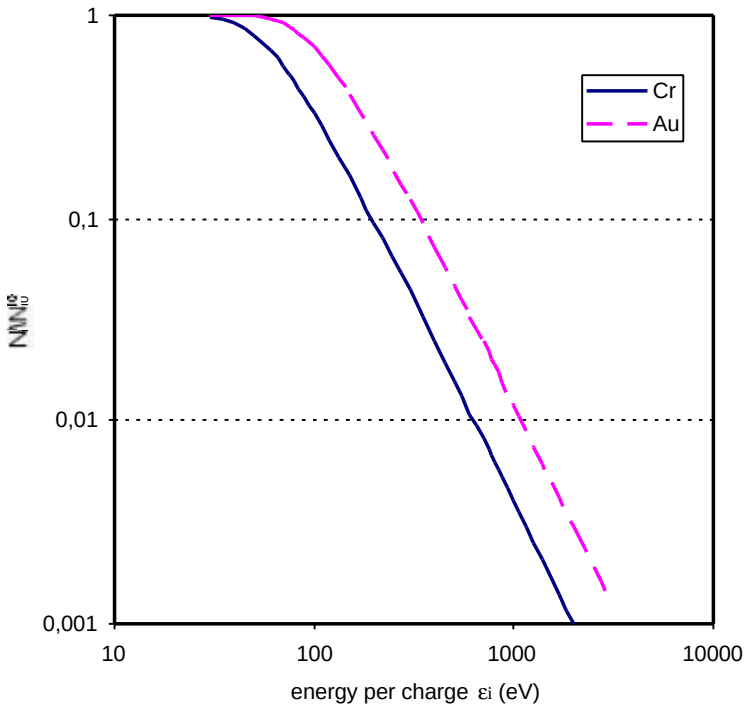


**Fig. 4 –** Coupling probability for oxygen plasma ($n_e$=4•10$^{12}$ cm$^{-3}$) and chromium and gold as injected ions, plotted vs. the energy per charge.

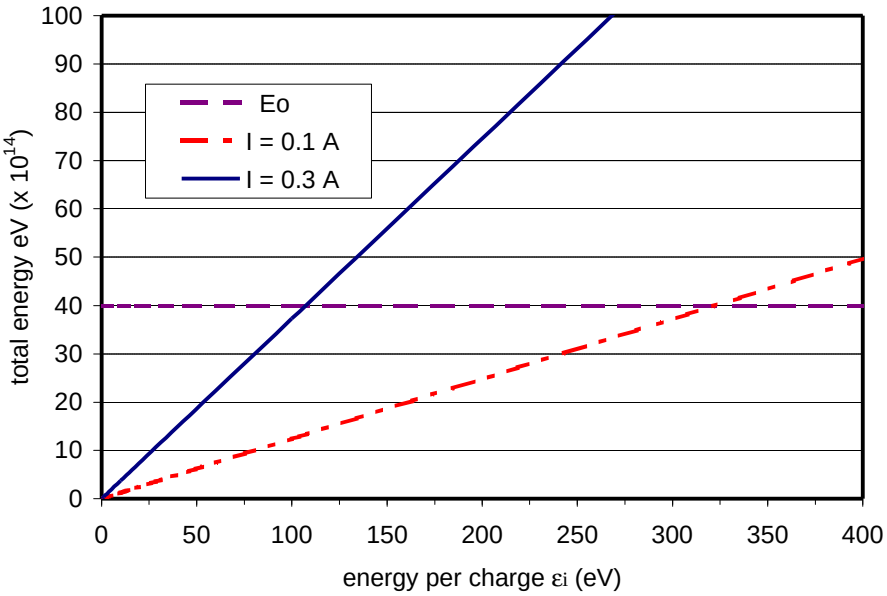


**Fig. 5 –** Comparison of the ion beam energy with the plasma ions' energy content.

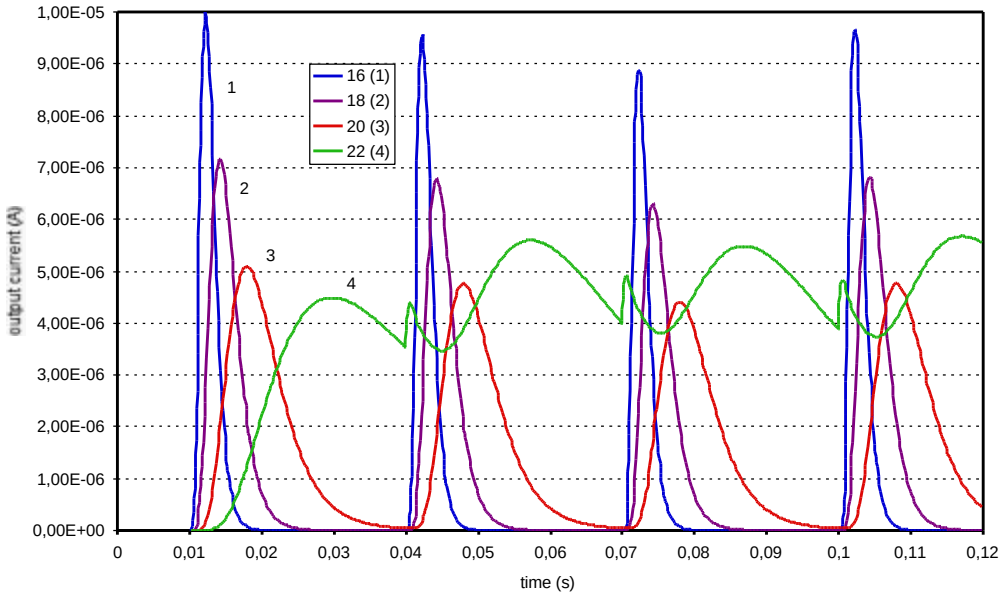


**Fig. 6 –** Chromium ion production vs. time as expected from the ECLISSE experiment.

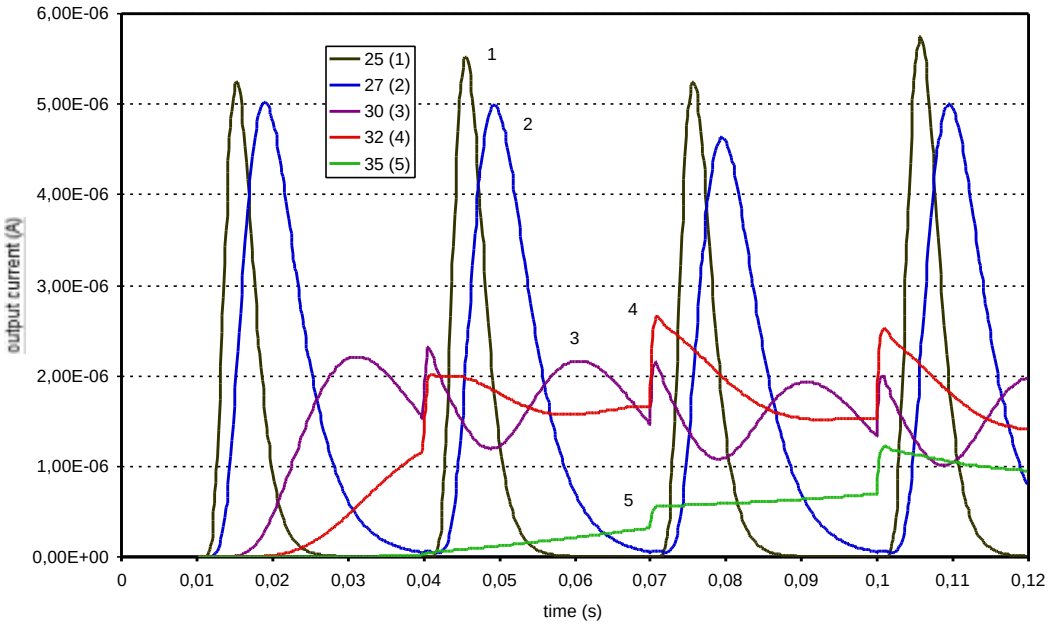


**Fig. 7 -** Rubidium ion production vs. time as expected from the ECLISSE experiment.

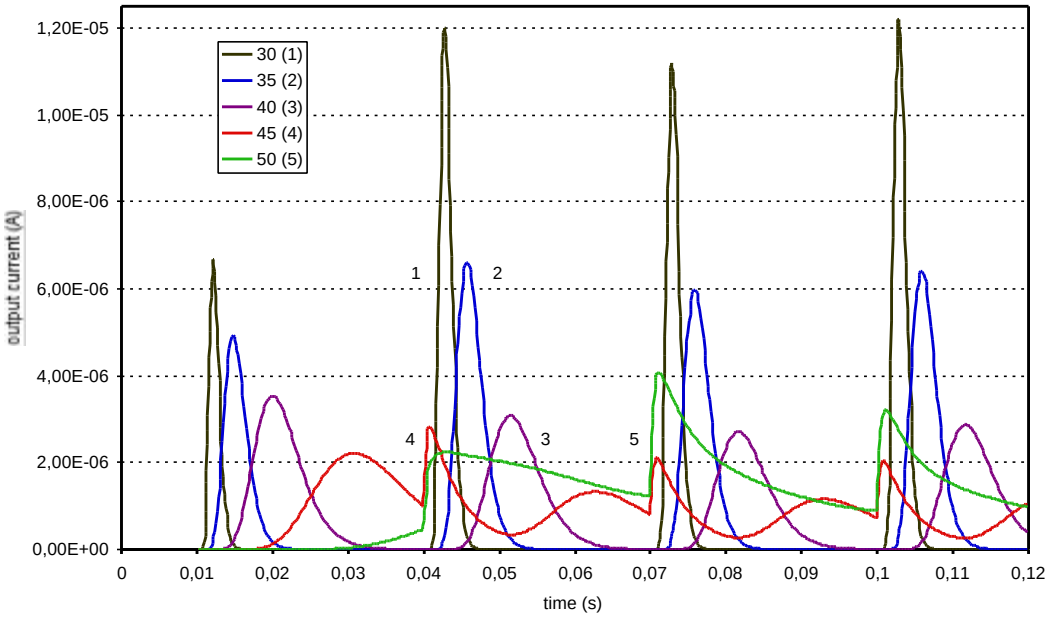


**Fig. 8 –** Gold ion production vs. time as expected from the ECLISSE experiment.

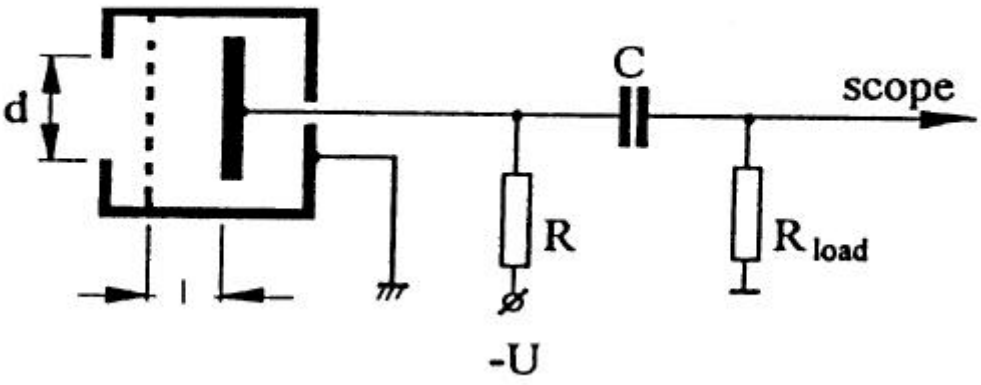


**Fig. 9** – The electrical scheme for the Ion Collector measurements.

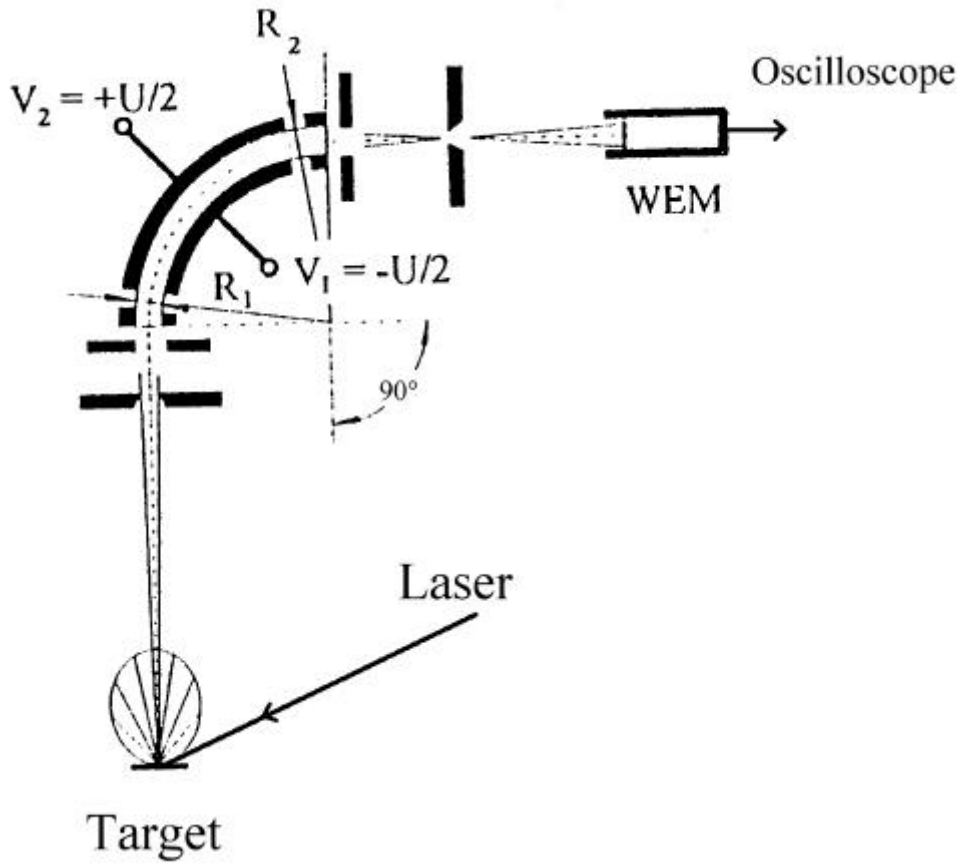


**Fig. 10** – The scheme of IEA [14].

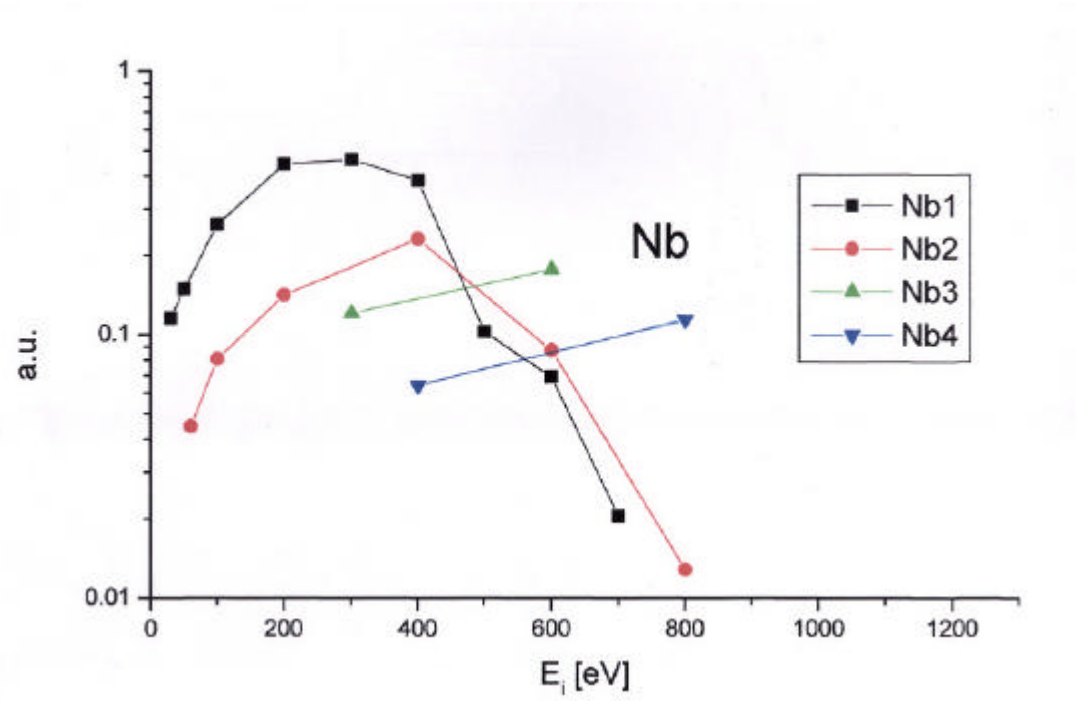


**Fig. 11** – Nb abundancies obtained from LIS operating at low laser energy (40 mJ).

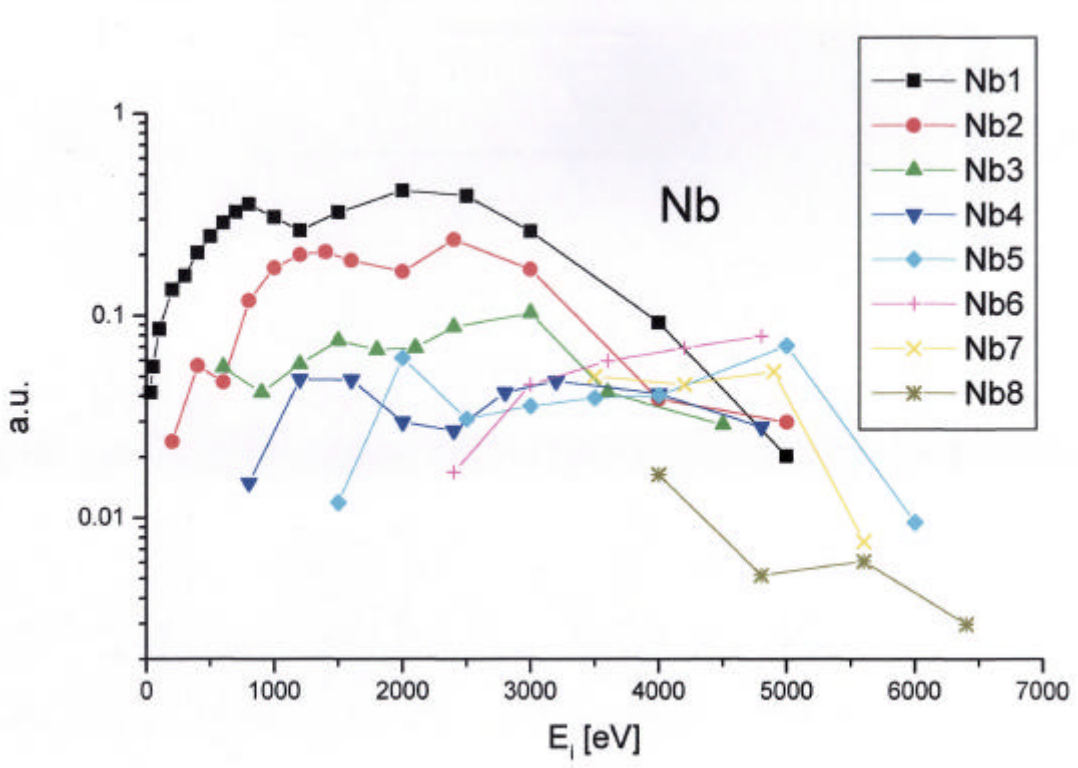


**Fig. 12** – Nb abundancies obtained from LIS operating at high laser energy (310 mJ).

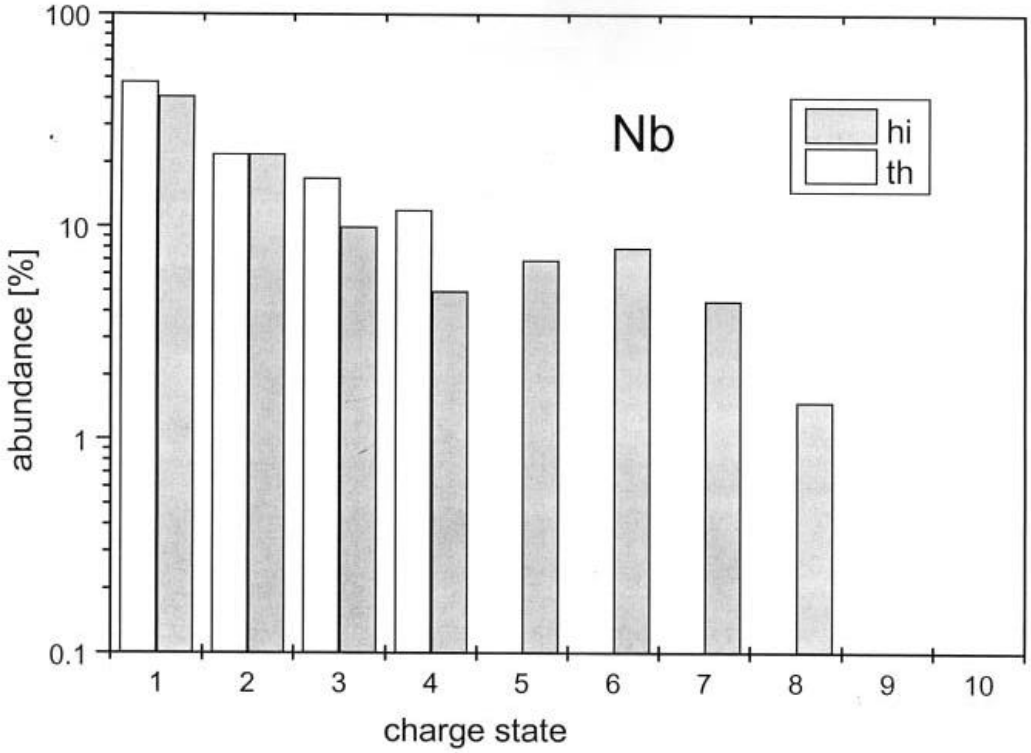


**Fig. 13** – Comparison of Nb abundancies obtained from LIS operating at threshold (30 mJ) and high laser energy (270 mJ).

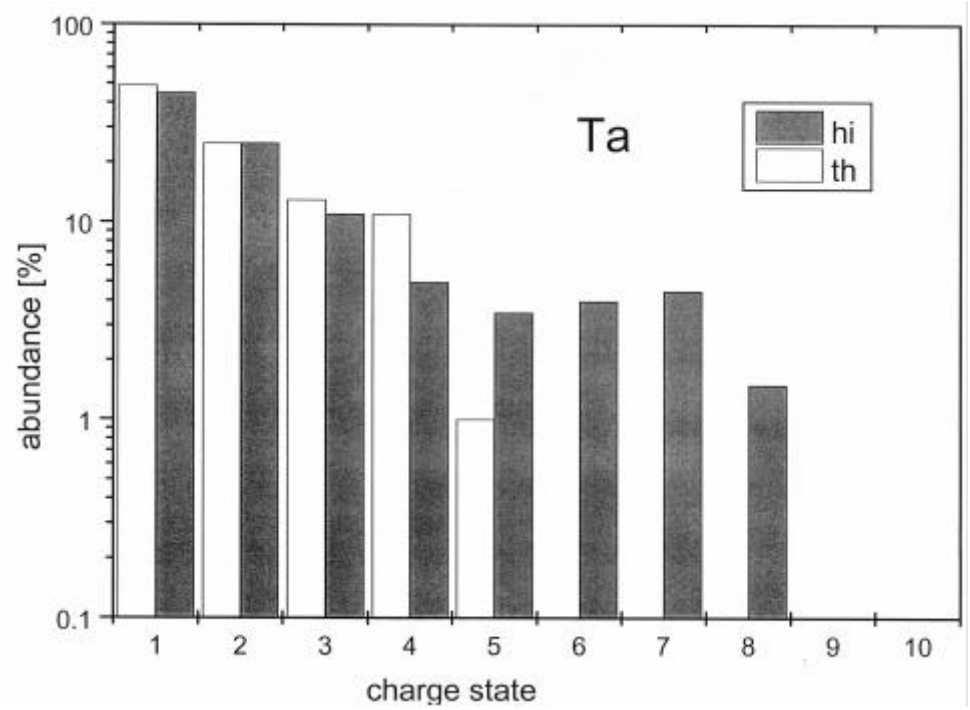


**Fig**. **14** – Comparison of Ta abundancies obtained from LIS operating at threshold (30 mJ) and high laser energy (310 mJ).

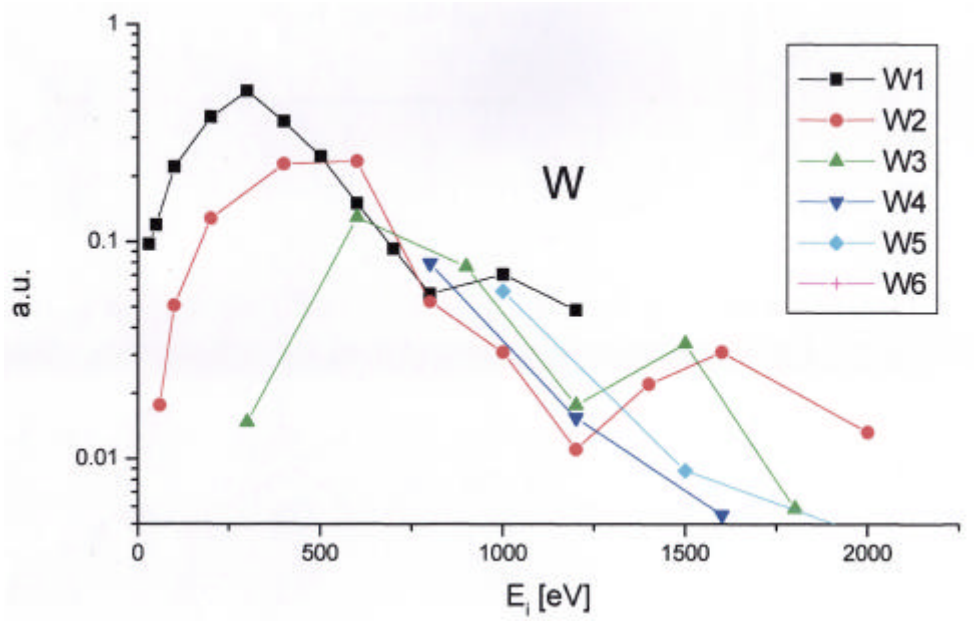


**Fig. 15** – W abundancies and energy distribution, as obtained from LIS operating at low laser energy (40 mJ).

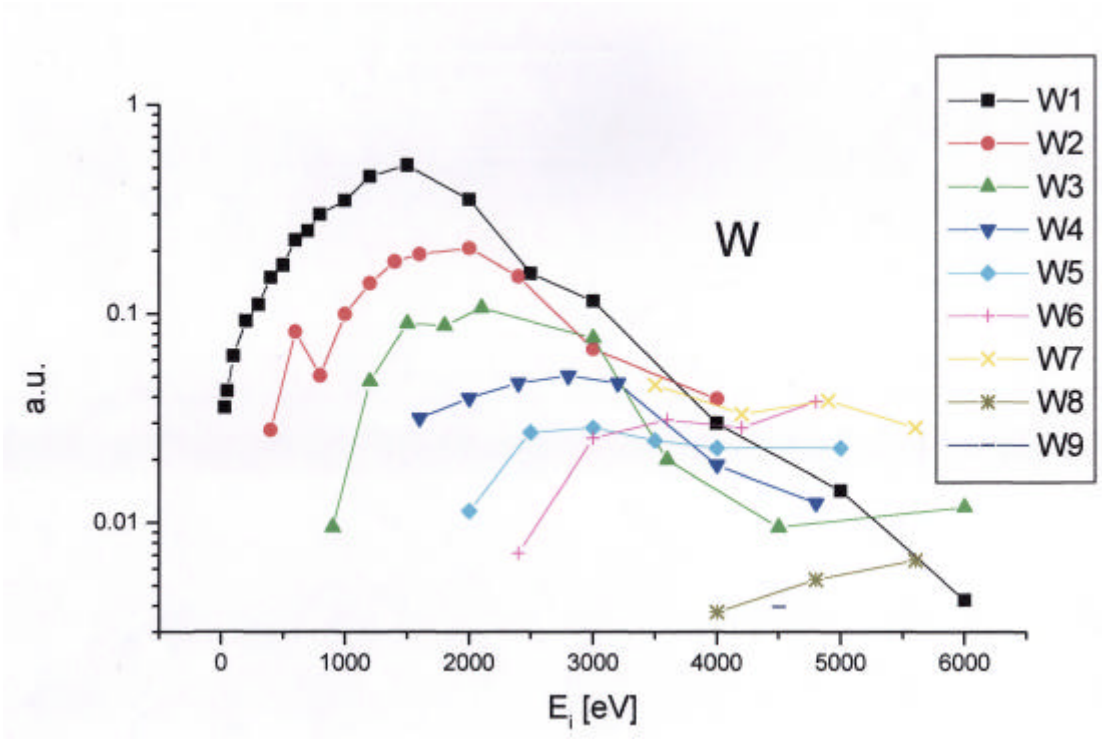


**Fig. 16** – W abundancies and energy distribution, as obtained from LIS operating at higher laser energy (310 mJ).

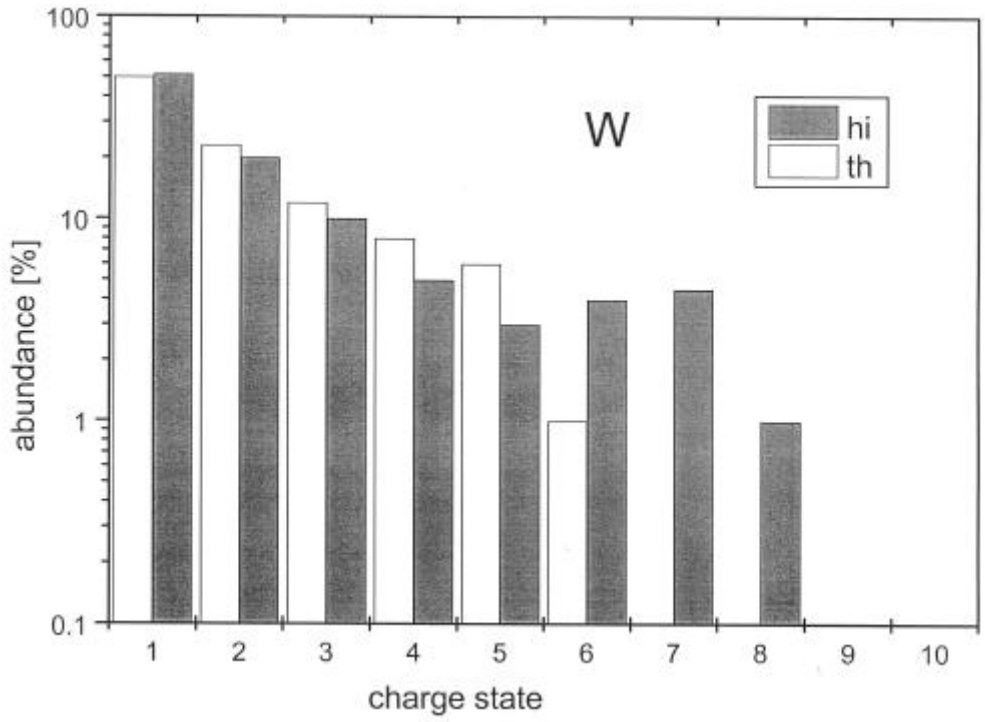


**Fig. 17** – Comparison of W abundancies obtained from LIS operating at threshold (40 mJ) and high laser energy (310 mJ).

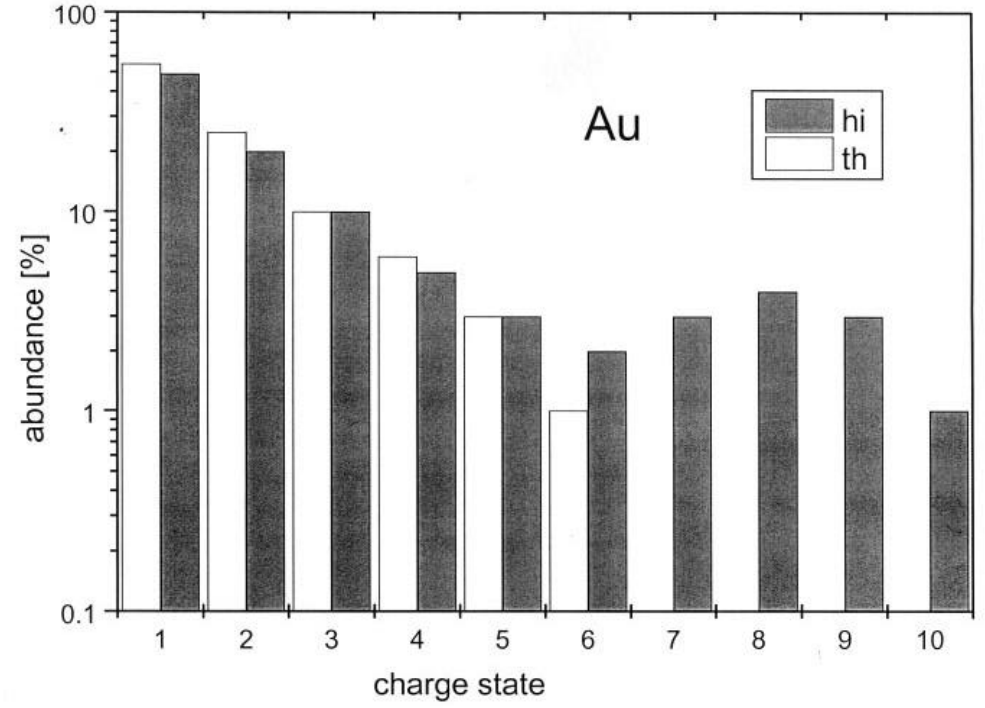


**Fig. 18** – Comparison of Au abundancies obtained from LIS operating at threshold (40 mJ) and high laser energy (310 mJ).

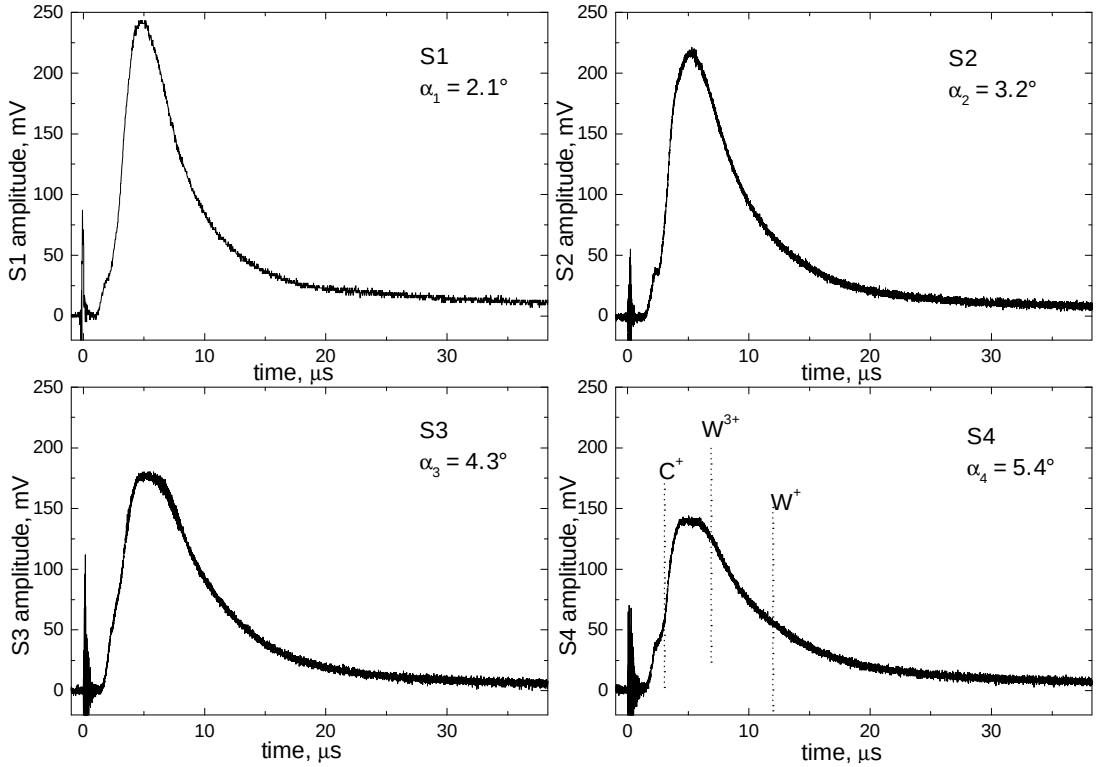


**Fig. 19**. S1-S4 ion collector signals recorded at different angles α to the target normal at $E_L$ = 1025 mJ (FP = 0, 1st laser shot onto fresh W target).

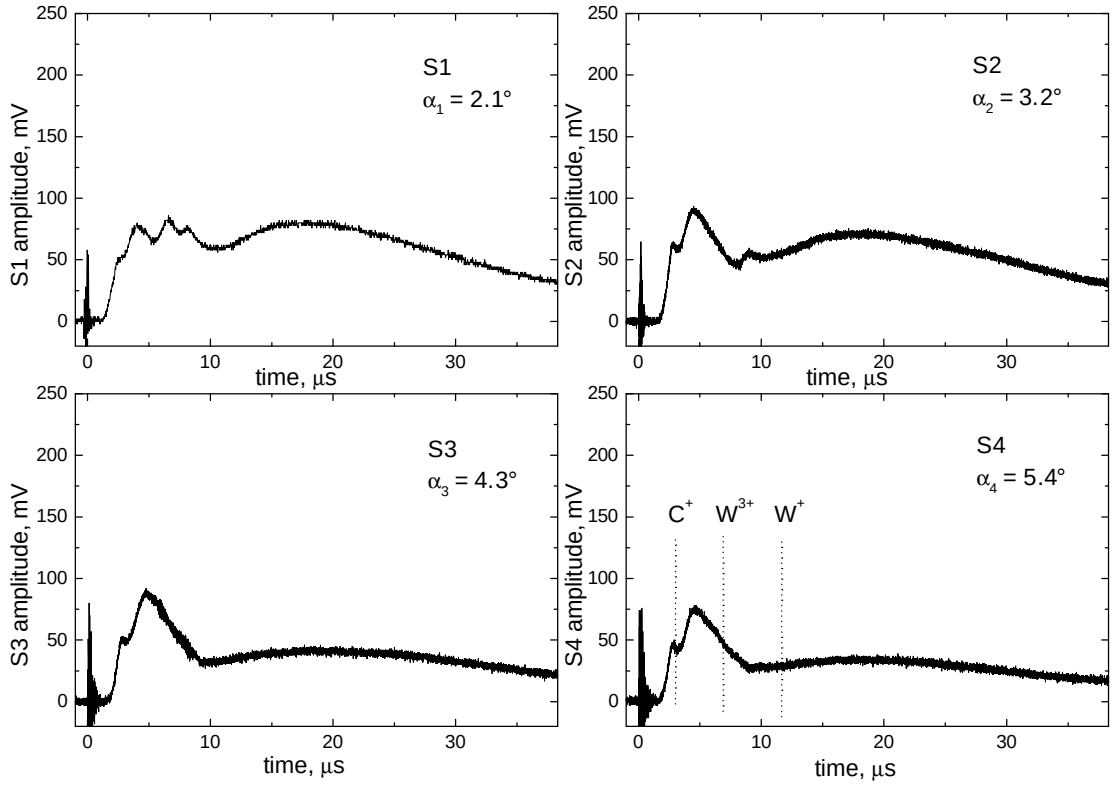


**Fig. 20**. S1-S4 ion collector signals recorded at different angles α to the target normal at $E_L$ = 1212 mJ (FP = 0, 2nd laser shot onto the same place as the shot in Figure 19).

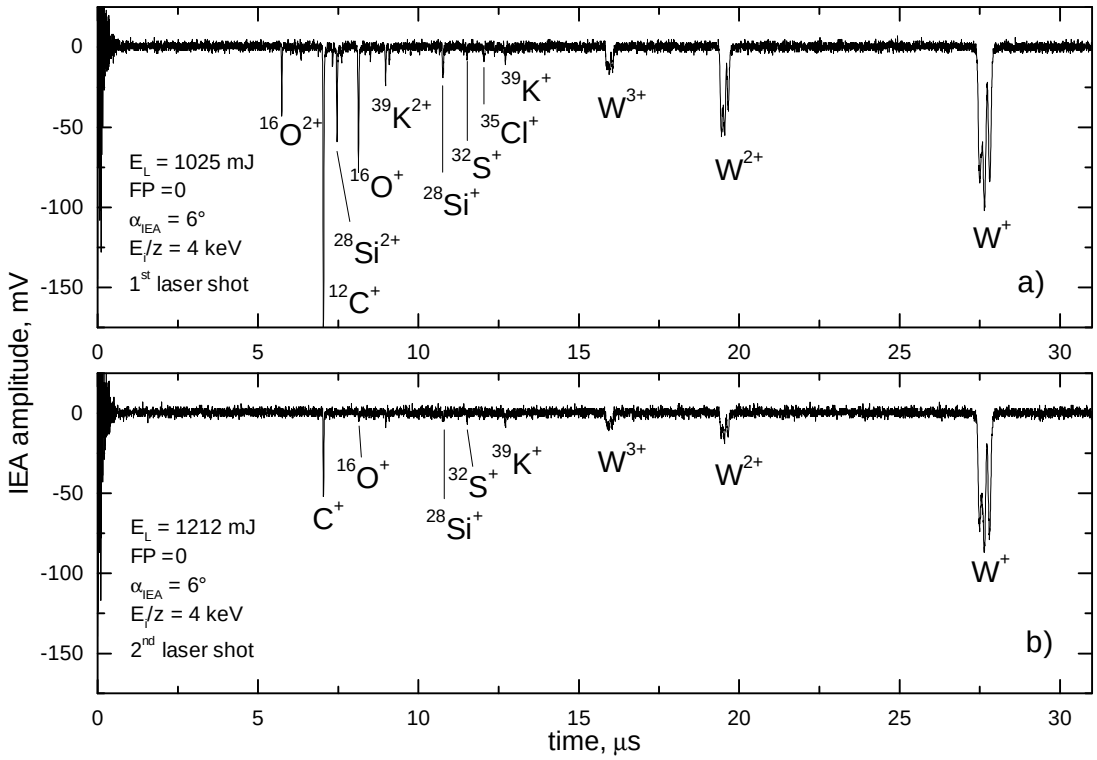


**Fig. 21**. Comparison of the IEA spectra of W plasma for laser shots discussed in Figures 19 and 20.

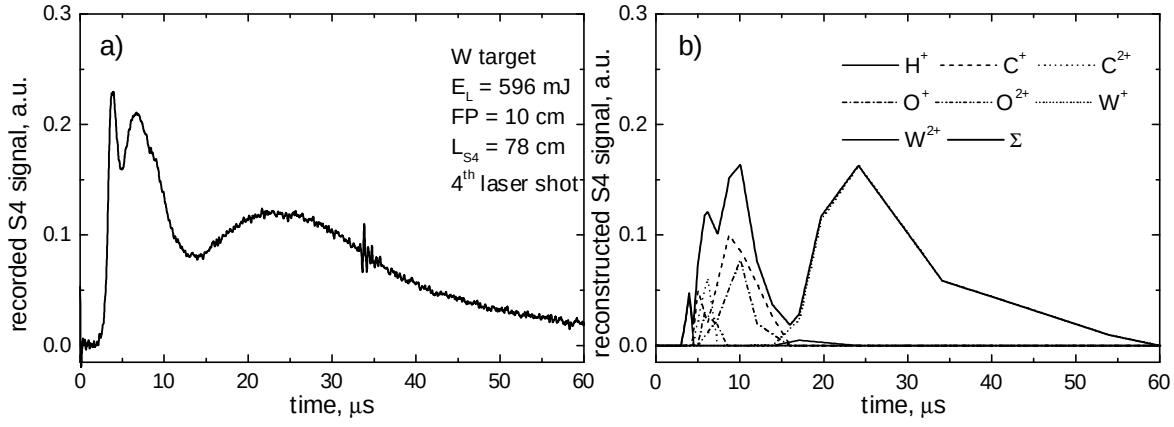


**Fig. 22**. Recorded (a) and reconstructed (b) S4 collector signal obtained on the basis of the IEA measurements.

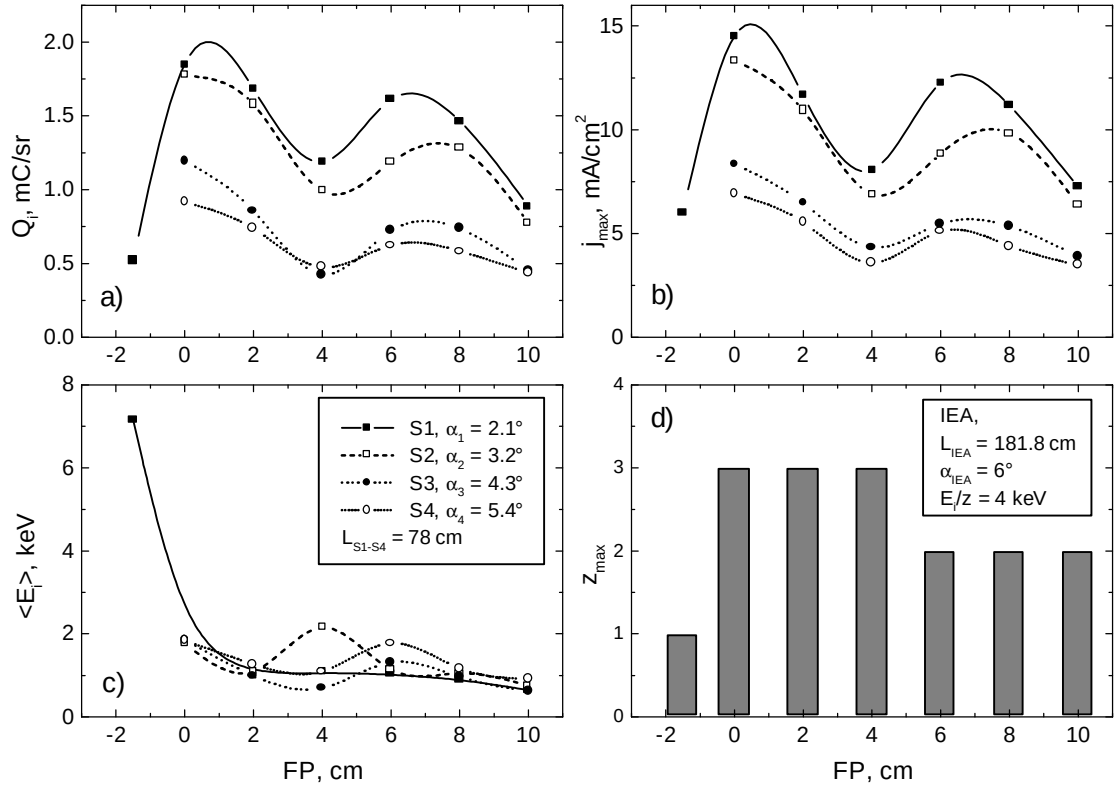


**Fig. 23**. Influence of the focus position on the charge carried by W ions, $Q_i$ (a), on the maximum ion current, $j_{max}$ (b), on the average ion energy, $<E_i>$ (c) and on the maximum charge state of W ions, $z_{max}$ (d).

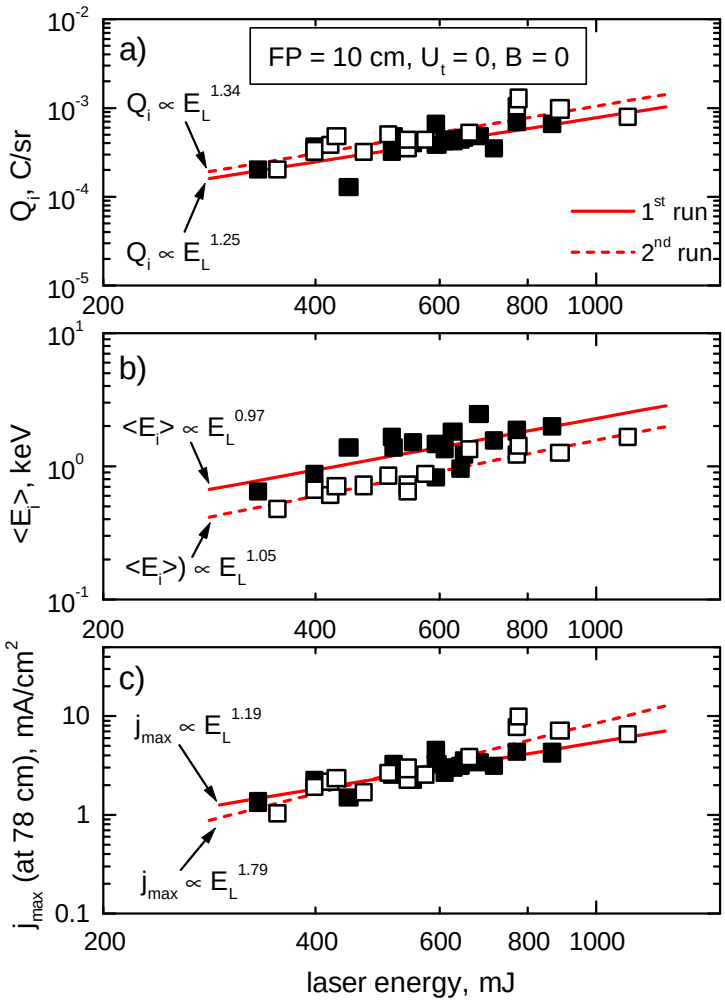


**Fig. 24**. Comparison of the total charge carried by W ions (a), of the average ion energy (b) and of the maximum ion current (c) of freely expanding W ion group.

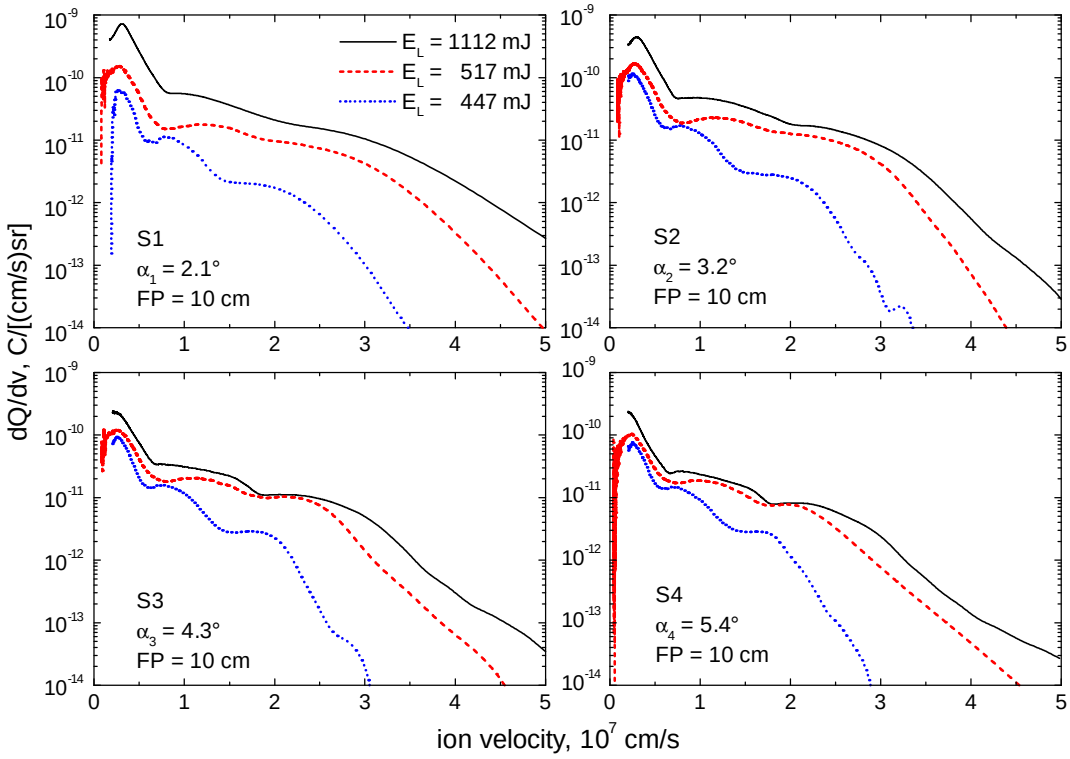


**Fig. 25**. Influence of the laser energy on the ion velocity distributions of freely expanding W plasma.

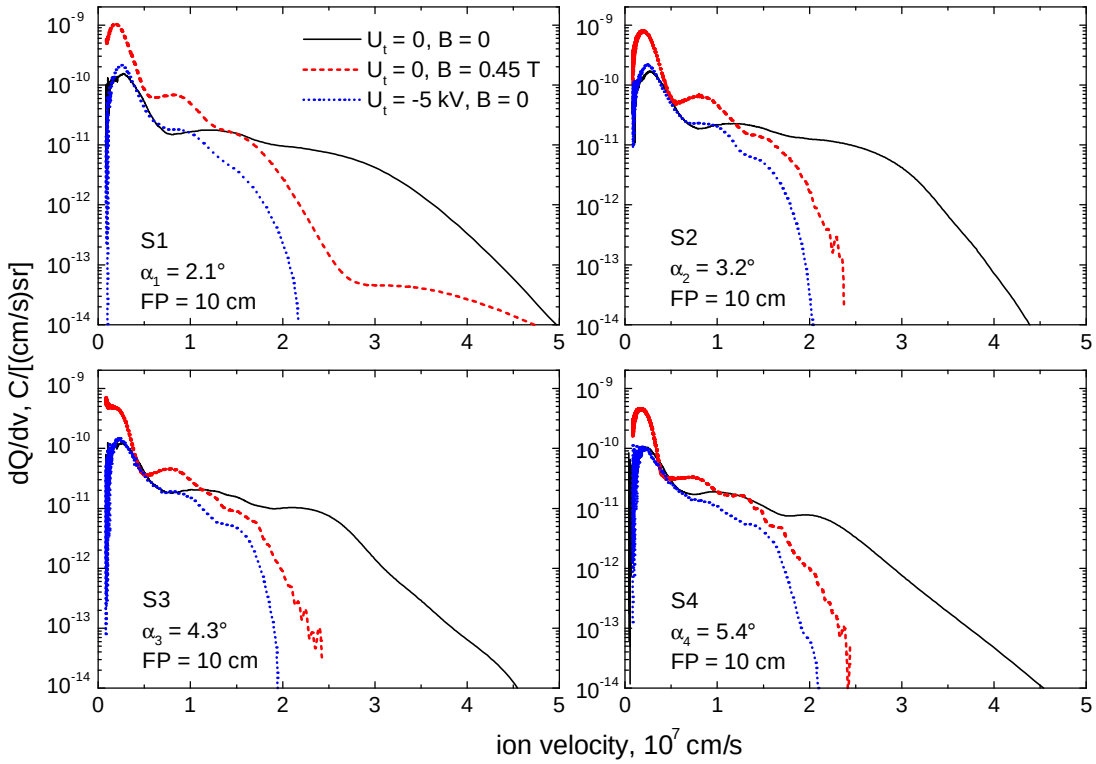


**Fig. 26**. Influence of external magnetic and electric fields on ion velocity distributions of W plasma ($E_L$ = 480±30 mJ).

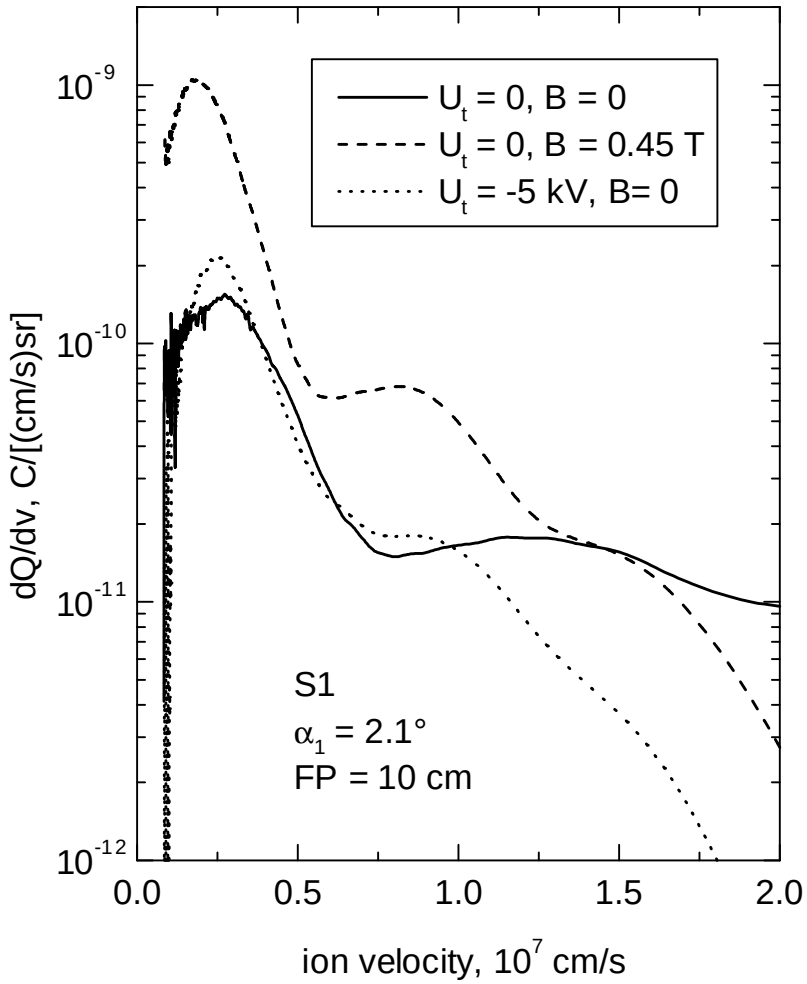


**Fig. 27**. Ion velocity distributions of W plasma in external magnetic and electric fields obtained from S1 collector (a part of Figure 26).

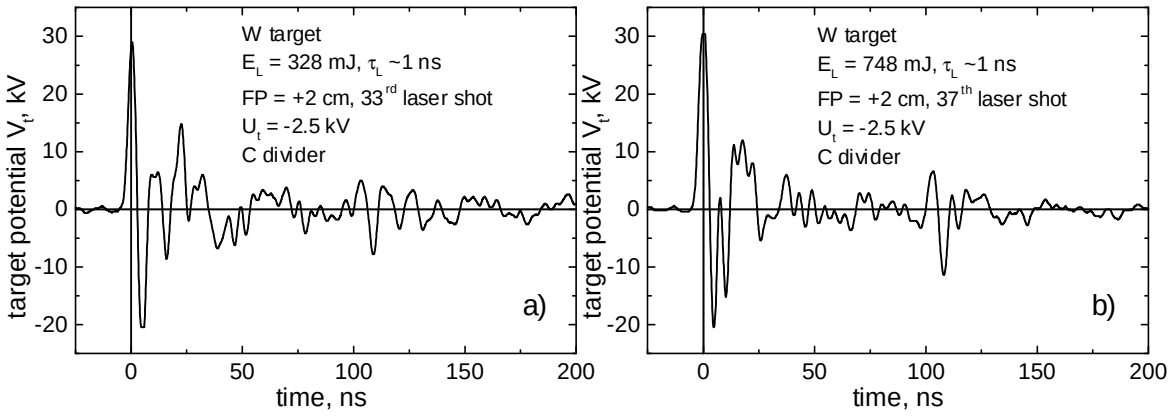


**Fig. 28**. Temporal dependence of the potential generated on the target (time = 0 corresponds to the laser pulse).

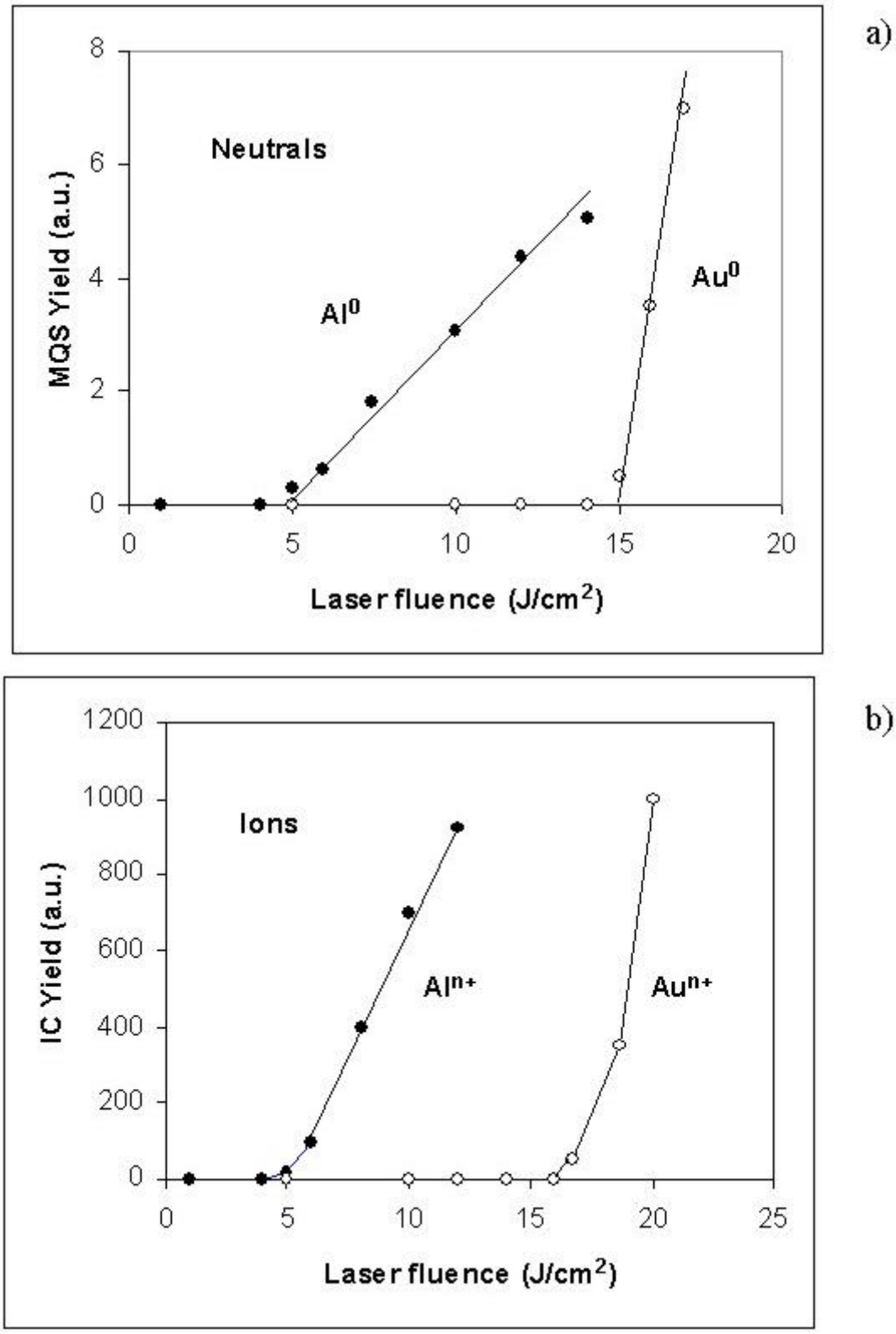


**Fig. 29** - Yield of neutrals (a) and ions (b) as a function of the laser fluence for aluminum and gold.

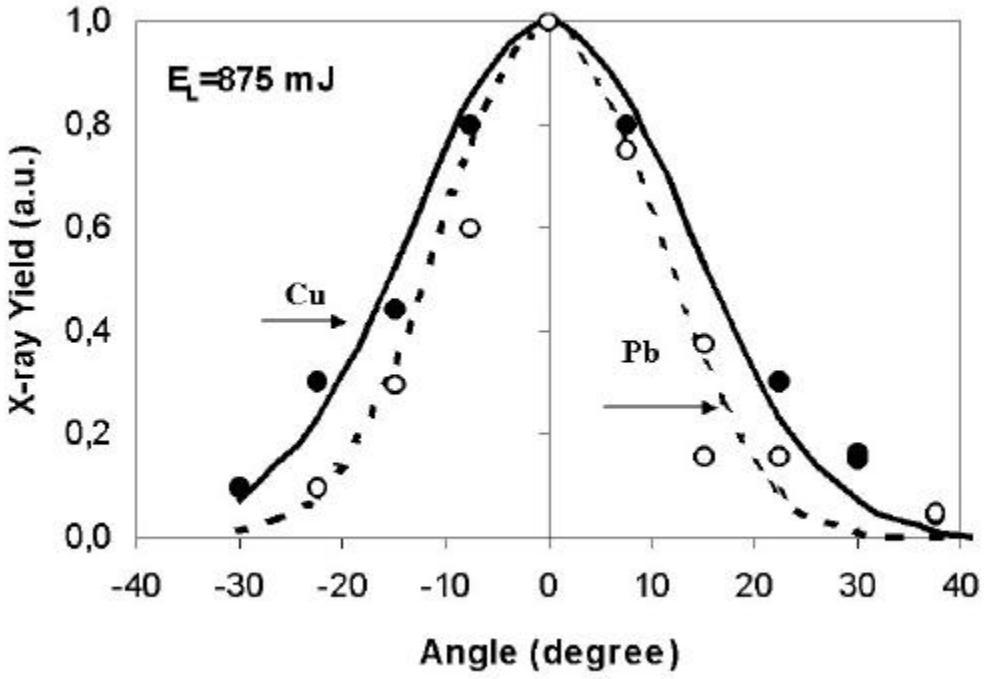


**Fig. 30**: Comparison of the angular distributions of thin films of Cu (solid circles) and Pb (open circles).

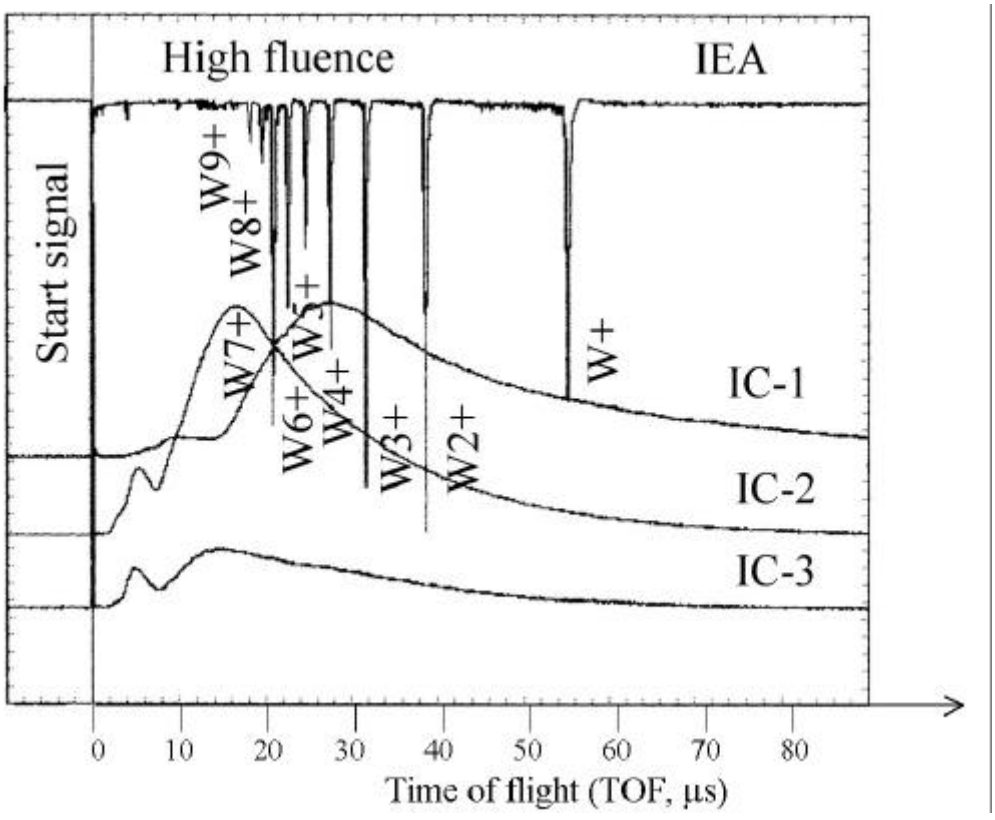


**Fig. 31**- Typical TOF spectrum for tungsten ions.

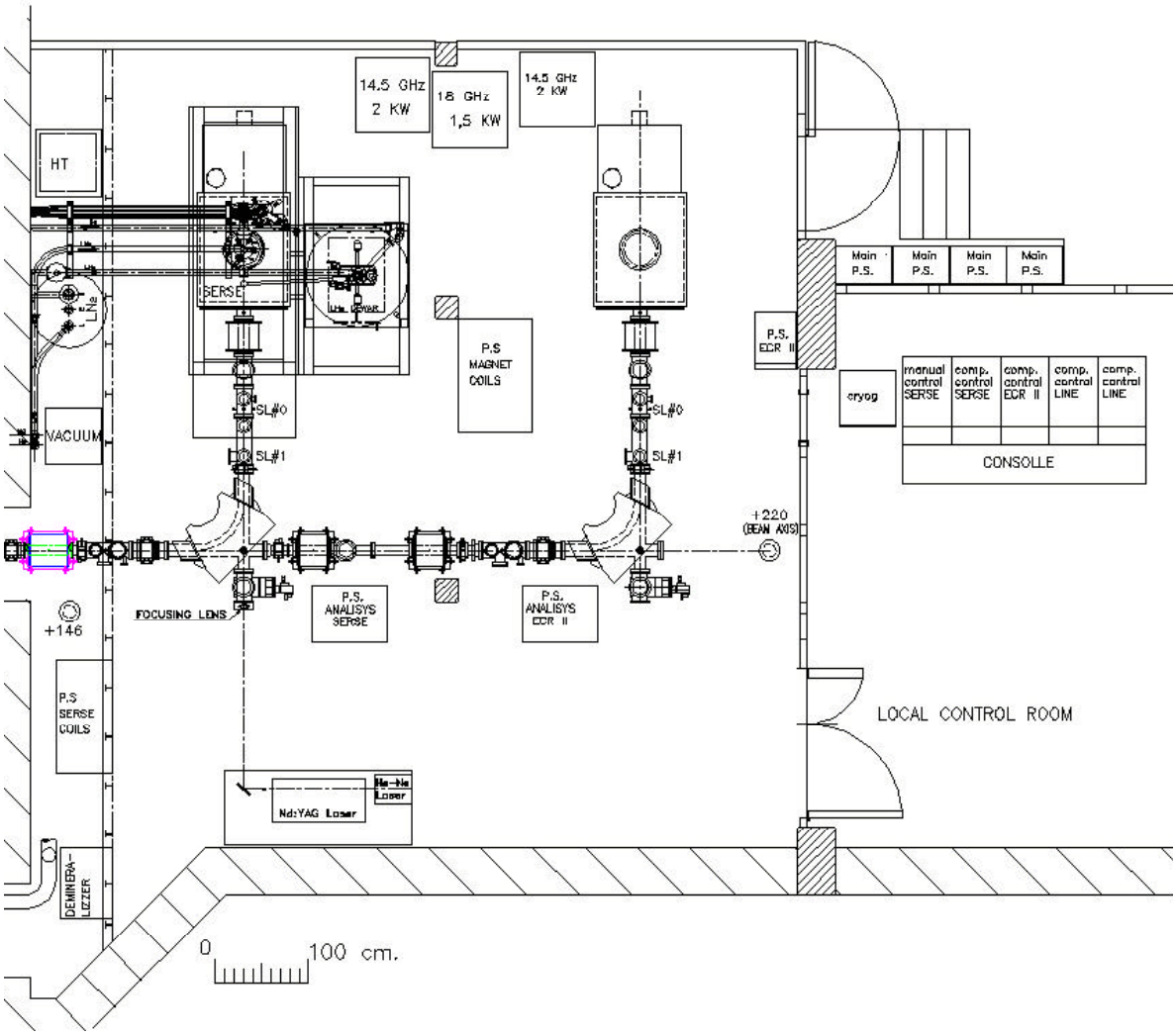


**Fig. 32** - A plan view of the experimental room.

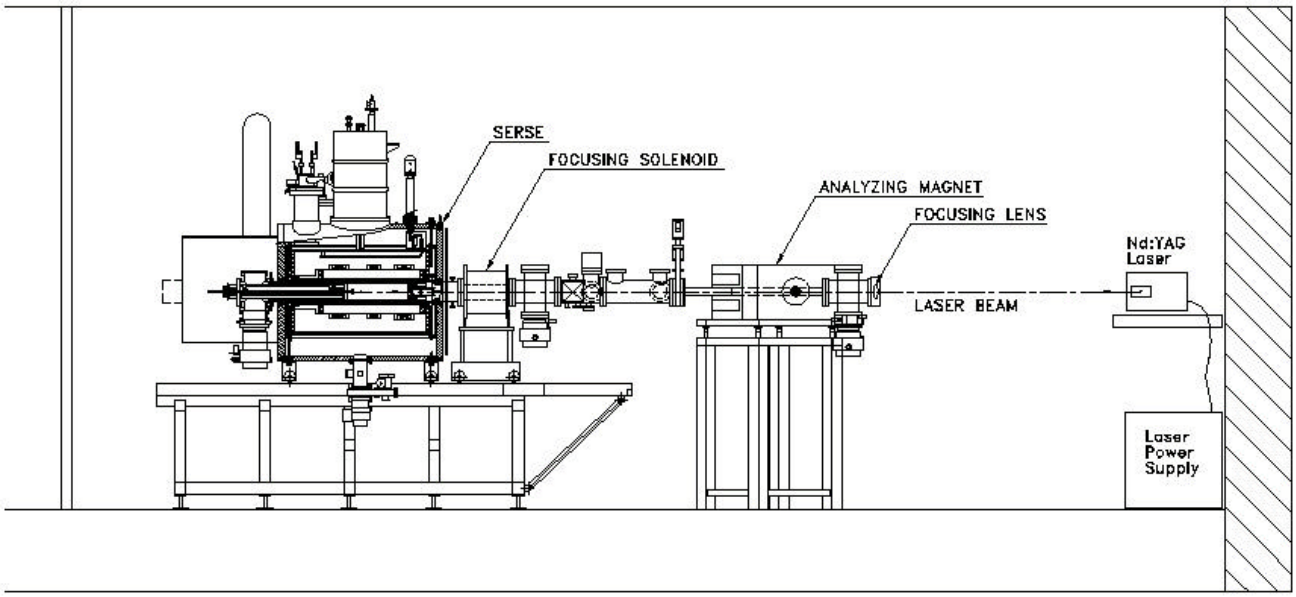


**Fig. 33 -** A side view of the experimental setup.

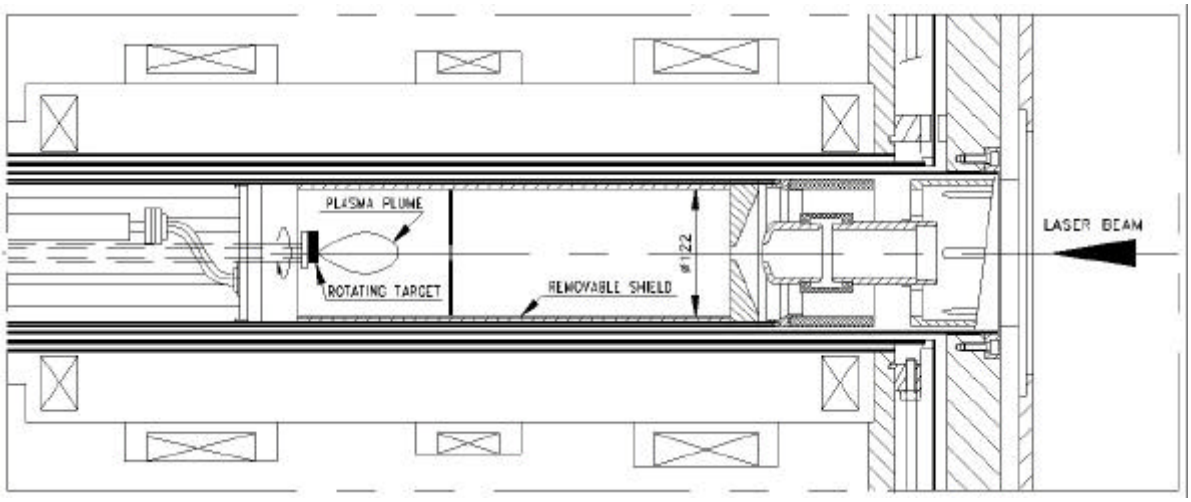


**Fig. 34** - A cross section of the plasma chamber.


**Fig. 35** - An Aluminum sample after 30 minutes of irradiation at 300 mJ, 30 Hz repetition rate.

| | |
|---|---|
| Laser type | Nd/YAg |
| Wavelength | 1064 nm |
| Pulse width | 9 ns |
| Pulse energy | 0÷900 mJ |
| Power density | $1 \cdot 10^{9} \div 5 \cdot 10^{10}$ W/cm$^2$ |
| Laser beam diameter | 10 mm |
| Laser beam divergence | < 0.7 mrad |
| Mode | Single shot/30 Hz repetition rate |

**Tab. 1**: The main features of the LIS at LNS, Catania.

| | |
|---|---|
| Superconducting wires | NbTi |
| LHe consumption | 4.5 l/h |
| Operating frequency | 18 GHz + 14.5 GHz |
| Type of launching | WR62, off-axis |
| B max (injection side) | 2.7 T |
| B min | 0.3 to 0.6 T |
| B max (extraction side) | 1.6 T |
| Resonance zone length | < 100 mm |
| Hexapole length | 700 mm |
| B rad (at chamber wall) | 1.55 T maximum |
| $\phi$plasma electrode | 12 mm |
| Extraction voltage | 30 kV max (20 kV typ.) |
| Biased disk | on axis, 300 to 700 V |
| Base pressure | 2 to $5 \cdot 10^{-8}$ mbar |
| Operational vacuum | 1 to $4 \cdot 10^{-7}$ mbar |
| Beamline pressure | lower than $1 \cdot 10^{-8}$ mbar |
| Emittance for HCI | 50 to 70 p mm.mrad |

**Tab. 2**: The main features of the SERSE source at LNS, Catania.

| | |
|---|---|
| Laser facility | Nd:glass |
| Pulse energy | $E_L \leq 1.5$ J |
| Pulse width | 1 ns |
| Wavelength | 1064 nm |
| Laser beam diameter | 20 mm |
| Laser beam divergence | ~ 0.5 mrad |
| Power density | $<10^{11}$ W/cm$^2$ |
| Focusing lens<br>Focus position vs. target surface | $f$ = 133.4 cm<br>$FP$ = –2-10 cm |
| Magnetic field (Helmholz coils) | $B_{max} \leq 0.45$ T |
| Target potential | $U_t$ = –5 to +15 kV |
| Operational vacuum | $p \sim 1\times10^{-6}$ Torr |

**Tab. 3**: The main features of the LIS at IPPLM, Warsaw.

| Elements | Al | Ti | Ni | Cu | Nb | Sn | Ta | W | Au | Pb |
|---|---|---|---|---|---|---|---|---|---|---|
| | | | | | | | | | | |
| Reflectivity | 0.97 | 0.85 | 0.87 | 0.98 | 0.70 | 0.85 | 0.80 | 0.79 | 0.99 | 0.88 |
| $E_{thrs}^{0}$ (neutral) (J/cm$^2$) | 0.15 | 0.36 | 0.65 | 0.17 | - | - | 1.00 | 1.31 | 0.15 | 0.10 |
| $E_{thrs}^{n+}$ (ion) (J/cm$^2$) | 0.14 | - | 0.52 | 0.17 | 1.00 | 0.55 | 0.67 | 1.40 | 0.16 | 0.60 |
| $E_o$ (theoretical) (J/cm$^2$) | 0.14 | 0.36 | 0.60 | 0.17 | 0.94 | 0.17 | 0.97 | 0.89 | 0.15 | 0.11 |
| $\Delta\Omega_T$ (sr) | 2.65 | 2.51 | 2.51 | 2.10 | 2.30 | 2.09 | 1.67 | 1.74 | 1.54 | 1.47 |
| $W_f = \Delta\Omega_T/\Delta\Omega_{IC}$ | 2650 | 2510 | 2510 | 2100 | 2300 | 2090 | 1670 | 1740 | 1540 | 1470 |

**Tab. 4**: Reflectivity and thresholds fluences of absorbed energy for neutrals and ions and comparison with the theoretical threshold values for ten different metals.

| Elements | Al | Ni | Nb | Sn | Ta | Au | Pb |
|---|---|---|---|---|---|---|---|
| | | | | | | | |
| Total emission, $N_t$ ($\bullet10^{14}$) | 6.9 | 22 | 21 | 8.5 | 18 | 6.0 | 9.0 |
| Ion emission, $N_i^{1+}$ ($\bullet10^{14}$) | 1.5 | 0.63 | 1.84 | 2.1 | 0.85 | 0.62 | 3.59 |
| Fractional ioniz., $N_i^{1+}/N_t$ (%) | 21.7 | 2.9 | 8.8 | 24.7 | 4.7 | 10.3 | 40 |
| Average velocity ($\bullet10^4$m/s) | 5.5 | 4.9 | 3.4 | 2.8 | 2.3 | 2.2 | 2.8 |
| Average kinetic energy (keV) | 0.42 | 0.73 | 0.55 | 0.47 | 0.50 | 0.49 | 0.81 |

**Tab. 5**: Total and ion emission, fractional ionization, average velocities and energies, measured at low laser fluences, for different metals.

| Elements | Al | Ni | Nb | Sn | Ta | Au | Pb |
|---|---|---|---|---|---|---|---|
| | | | | | | | |
| Total emission, $N_t$ ($\bullet 10^{14}$) | 23 | 50 | ~ 120 | - | 40 | 34 | ~ 180 |
| Ion emission, $N_i^{1+}$ ($\bullet 10^{14}$) | 12 | 10 | - | 6.3 | 8 | 11 | - |
| Fractional ioniz., $N_i^{1+}/N_t$ (%) | 52 | 20 | - | - | 20 | 32 | - |
| Average velocity ($\bullet 10^4$m/s) | 9.8 | 6.3 | 5.5 | 4.4 | 3.7 | 3.7 | 2.9 |
| Average kinetic energy (keV) | 1.34 | 1.2 | 1.46 | 1.19 | 1.28 | 1.4 | 0.92 |

**Tab. 6**: Total and ion emission, fractional ionization, average velocities and energies, measured at high laser fluences, for different metals.